ACS Infectious Diseases

pubs.acs.org/journal/aidcbc Article

Searching for Antipneumococcal Targets: Choline-Binding Modules as Phagocytosis Enhancers

Emma Roig-Molina, Manuel Sánchez-Angulo, Jana Seele, Francisco García-Asencio, Roland Nau, Jesús M. Sanz,*,▽ and Beatriz Maestro*,▽

Cite This: ACS Infect. Dis. 2020, 6, 954–974 Read Online

ACCESS | Metrics & More | Article Recommendations | Supporting Information

ABSTRACT: Choline-binding proteins (CBPs) from *Streptococcus pneumoniae* comprise a family of modular polypeptides involved in essential events of this pathogen. They recognize the choline residues present in the teichoic and lipoteichoic acids of the cell wall using the so-called choline-binding modules (CBMs). The importance of CBPs in pneumococcal physiology points to them as novel targets to combat antimicrobial resistances shown by this organism. In this work we have tested the ability of exogenously added CBMs to act as CBP inhibitors by competing with the latter for the binding to the choline molecules in the bacterial surface. First, we carried out a thorough physicochemical characterization of three native CBMs, namely C-LytA, C-Cpl1, and C-CbpD, and assessed their affinity for choline and macromolecular, pneumococcal cell-wall mimics. The interaction with these substrates was evaluated by molecular modeling, analytical ultracentrifugation, surface plasmon resonance, and fluorescence and circular dichroism spectroscopies. Van't Hoff thermal analyses unveiled the existence of one noncanonical choline binding site in each of the C-Cpl1 and C-CbpD proteins, leading in total to 5 ligand-binding sites per dimer and 4 sites per monomer, respectively. Remarkably, the binding affinities of the CBMs do not directly correlate with their native oligomeric state or with the number of choline-binding sites, suggesting that choline recognition by these modules is a complex phenomenon. On the other hand, the exogenous addition of CBMs to pneumococcal planktonic cultures caused extensive cell-chaining probably as a consequence of the inhibition of CBP attachment to the cell wall. This was accompanied by bacterial aggregation and sedimentation, causing an enhancement of bacterial phagocytosis by peritoneal macrophages. In addition, the rational design of an oligomeric variant of a native CBM led to a substantial increase in its antibacterial activity by multivalency effects. These results suggest that CBMs might constitute promising nonlytic antimicrobial candidates based on the natural induction of the host defense system.

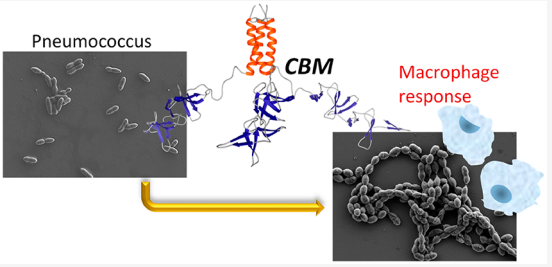

KEYWORDS: *Streptococcus pneumoniae, choline-binding proteins, magnetic nanoparticles, antimicrobial resistance, DEAE, bacterial cell wall*

INTRODUCTION

Streptococcus pneumoniae (pneumococcus) is a Gram-positive bacterium responsible for acute life-threatening infections including meningitis and sepsis,[1] and it constitutes the most frequently detected bacterial pathogen in cases of community-acquired pneumonia.[2] Moreover, it is a major causative agent of otitis media and sinusitis.[3] Pneumococcal diseases are widespread both in industrialized and in developing countries, leading to about 1.2 million deaths per year according to the World Health Organization (WHO), 70% of which correspond to children under 5 and elderly adults above 70 years old.[4] Furthermore, *S. pneumoniae* is considered by the WHO as a priority pathogen for R&D of new antibiotics[5] and as a "serious" threat by the U.S. Department of Health.[6]

Current intervention strategies against pneumococcal disease, based on vaccination and antibiotic treatment, face several drawbacks. Present-day vaccination only covers part of the nearly 100 serotypes already described for this pathogen,[7] and the immunogenic effect of the available vaccines may be limited in some cases,[8] while serotype replacement phenomena are also frequently reported[9,10] leading to resurgent disease.[11] Besides, vaccines do not always protect in developing countries, either because nonvaccine serotypes predominate or due to insufficient access to the vaccination programmes.[12,13] On the other hand, antimicrobial resistance constitutes a serious concern: appearance of new non-susceptible pneumococcal strains to β-lactam and/or macrolid antibiotics is commonly reported,[14,15] reaching resistance levels of *ca.* 50% in some European countries.[16] This situation

Received: September 10, 2019
Published: March 5, 2020

https://dx.doi.org/10.1021/acsinfecdis.9b00344
ACS Infect. Dis. 2020, 6, 954–974

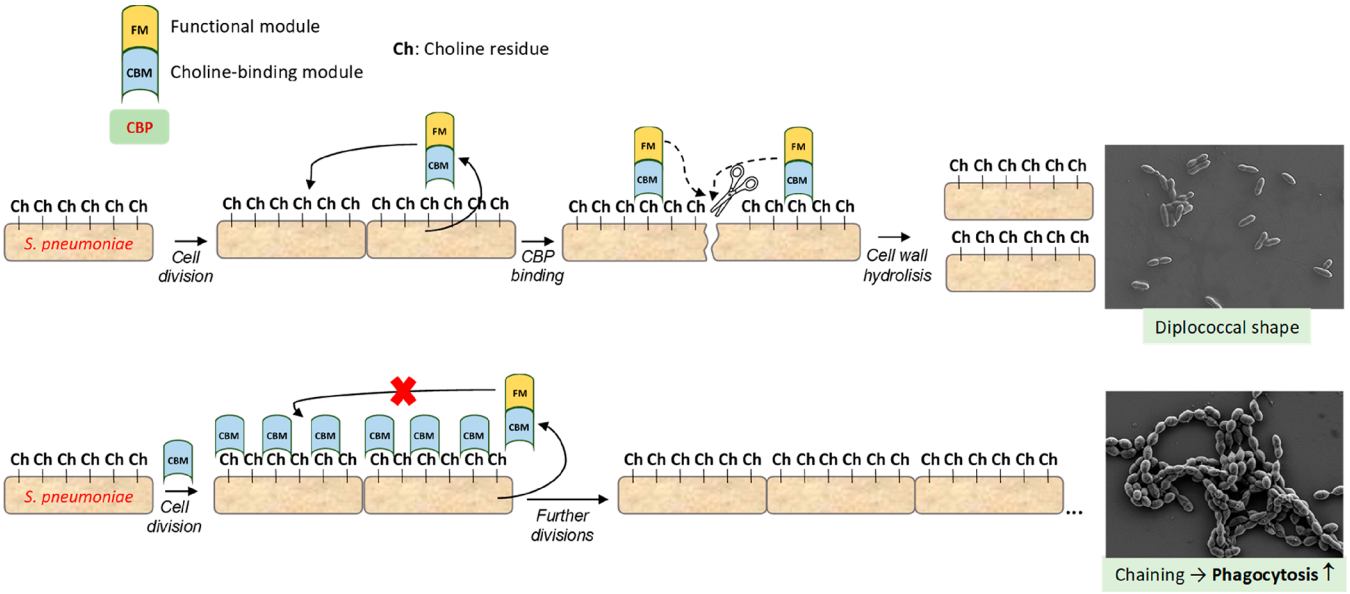

Figure 1. Strategy for the use of CBMs as nonlytic antipneumococcal molecules. Under usual growth conditions, cells divide and then activate full-length CBP hydrolases such as LytA and LytB that bind to choline residues in the teichoic acids and carry out the selective hydrolysis of the cell wall leading to the separation of daughter cells. On exogenous addition of CBMs, CBP hydrolases cannot attach to the cell wall as all choline sites are occupied, so daughter cells do not separate upon division, leading to cell chaining which hampers infectivity and promoting pathogen removal by phagocytosis.

makes necessary the research on new effective chemotherapies involving distinctive mechanisms.

The cell wall of *S. pneumoniae*, and especially the proteins attached to its surface, constitute an attractive antimicrobial target to develop new drugs. Three main groups of surface proteins in pneumococcus have been described, namely (i) lipoproteins, (ii) choline-binding proteins (CBPs), and (iii) LPXTG-sequence-containing proteins, with the latter being covalently attached to the peptidoglycan.[17] Among them, CBPs represent a family of 13−16 members, depending on the strain, that are involved in several essential processes of this pathogen, *e.g.* cell-wall hydrolysis prior to daughter cell separation upon division and release of virulence factors (LytA, LytB, LytC), adhesion to the host (PspC), bacterial fratricide (LytA, LytC, CbpD), or evasion from the immune system (LytA, PspA, PspC).[18] Furthermore, these proteins are highly conserved among all serotypes and recognize the choline moieties present in the cell wall teichoic and lipoteichoic acids, allowing their noncovalent adsorption to the macromolecular peptidoglycan structure by means of a choline-binding module (CBM).[18] The CBMs differ, among themselves, in size, oligomeric state, and position in the protein (N- or C-termini), but all of them consist of a variable number of aromatic-rich motifs, about 20 residues long, termed choline-binding repeats (CBRs). These CBRs belong to the widespread CW_binding 1_motif family (PFAM code PF01473) (http://pfam.xfam.org/family/PF01473) and are structurally formed by a ≈14-aa β-hairpin followed by a ≈6-aa linker. The choline-binding modules are three-dimensionally arranged in a β,β-3 solenoid superstructure, generating a choline-binding site between any two consecutive CBRs and in which the ligand is primarily stabilized by cation−π and van der Waals interactions with the aromatic side chains.[18]

Taking into account the variety of roles carried out by the CBPs (as involved in all key aspects of the pneumococcal vital cycle), several efforts have been carried out to inhibit choline recognition and hence to displace CBPs from the cell surface. Exogenously added free choline is a long known CBP inhibitor, competing with those molecules present in the teichoic acids on binding to the protein.[19,20] As a result, daughter cell separation is hampered, leading to the appearance of long cellular chains.[20] However, the poor affinity of CBPs for the free ligand[21−25] makes necessary the use of millimolar concentrations of this compound, which are therapeutically not achievable. Nevertheless, choline binding affinity to CBPs increases exponentially by using multivalent nanoparticles such as choline dendrimers which inhibit the CBPs activity *in vitro* around 10,000-fold more efficiently than free choline, interfering with daughter cell separation after division[26] and favoring phagocytosis of the cell chains by microglial cells.[27]

Induction of host phagocytosis may constitute an interesting way to find novel therapies. Some widely used molecules, for instance lytic β-lactam antibiotics, have been shown to induce the release of inflammatory and damaging toxins such as pneumolysin in contrast to nonlytic antimicrobials. The use of nonlytic antibacterials appears to be beneficial in experimental models in comparison with β-lactam antibiotics. Limited clinical data suggest that this approach may also be beneficial in human infections with a high bacterial load.[28,29] Moreover, release of intracellular content by autolysis has been described to interfere with the normal host phagocytic system.[30] This prompted us to further investigate alternative mechanisms of CBP inhibition that do not involve cell lysis. In this sense, we had previously found that complexing the choline residues in the cell wall with isolated CBMs such as C-LytA and C-Cpl1 (derived from the bacterial autolysin LytA and the phagic lysozyme Cpl1, respectively) resulted in the inhibition of the enzymatic activity *in vitro* of their full parental enzymes (LytA and Cpl1) which then would not be capable to reach their targets.[31]

Based on these preliminary results, we decided to further develop the idea of using isolated CBMs as nonlytic

https://dx.doi.org/10.1021/acsinfecdis.9b00344
ACS Infect. Dis. 2020, 6, 954−974

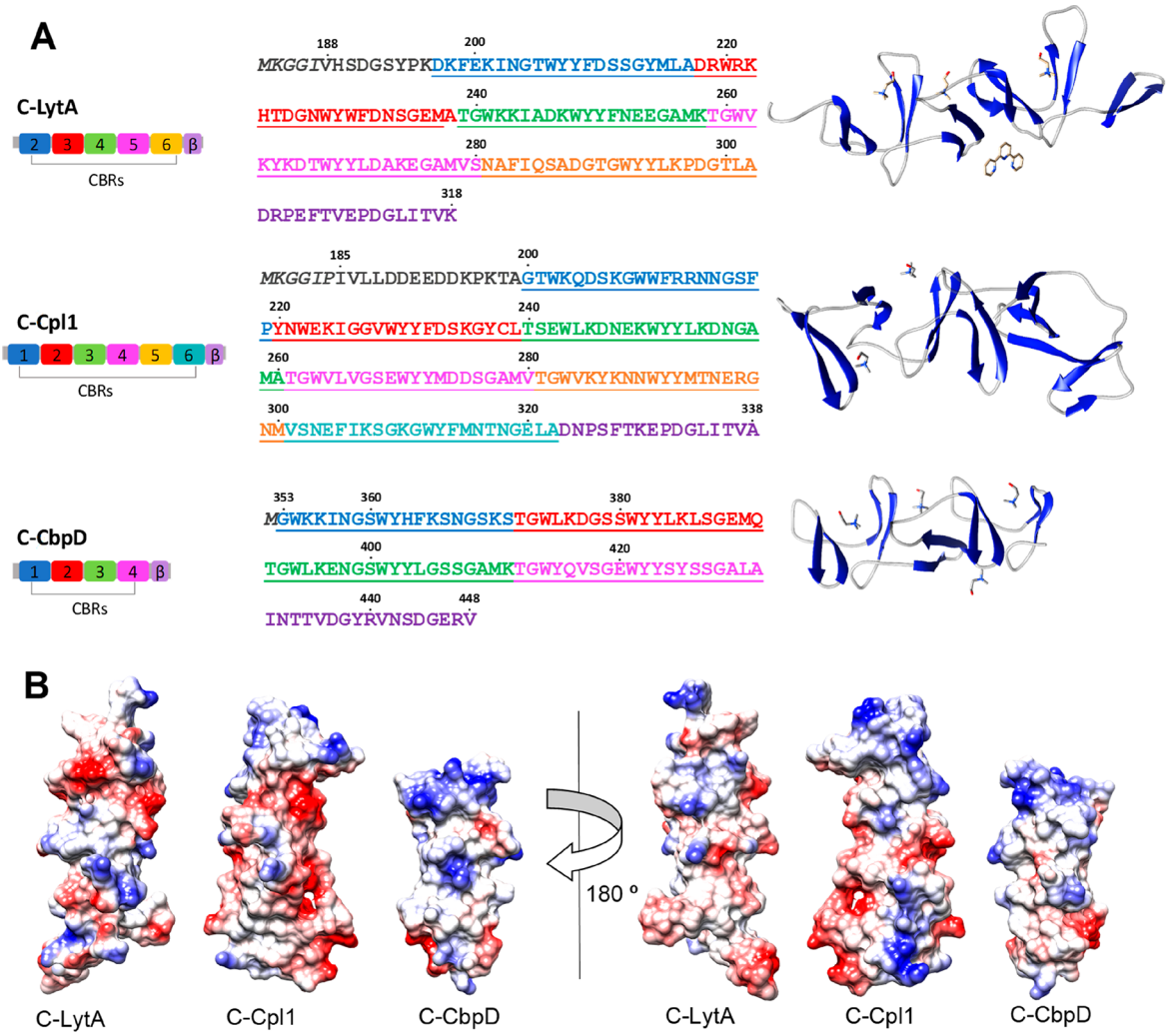

Figure 2. (A) Amino acid sequence of CBMs used in this study, indicating the numbered CBRs and the C-terminal tail, together with a secondary structure representation. Choline or choline analogs in the binding sites are displayed in stick representation. Residues in italics do not belong to the native parental sequence. CBR and amino acid numbering scheme is that of the parental CBP. (B) Three-dimensional surface representation with Coulombic coloring (red indicates negative polarity, blue indicates positive polarity, white indicates zero polarity). C-LytA and C-Cpl1 are represented by their crystallographic structures (PDB codes 1HCX and 1OBA, respectively) whereas C-CbpD is represented by a homology model with docked choline molecules (see text). Figures were rendered with UCSF Chimera 1.10.[74]

antipneumococcal molecules to bind to the choline residues on the pneumococcal surface, making them unable to be recognized by parental, full-length CBPs. Our strategy is shown in Figure 1. Among other effects, CBM-mediated inhibition of peptidoglycan hydrolases such as LytA and LytB should hamper daughter cell separation upon division, leading to chain formation and eventually favoring the phagocytosis of the chains, similarly to addition of choline and choline dendrimers.[27,32] To this aim we have carried out a biophysical characterization of three CBMs differing in number of CBRs and oligomeric state, namely C-LytA, C-CbpD, and C-Cpl1, which belong to the bacterial host LytA and CbpD proteins and the pneumococcal Cpl-1 phage-encoded lysozyme, respectively. The LytA amidase is the major murein hydrolase of *S. pneumoniae*, and its C-terminal module (C-LytA) is the best studied species of the CBM family[22,33,34] (PDB code: 1HCX). On the other hand, CbpD is a murein hydrolase that assists in cellular fratricide together with LytA, LytC, and CibAB.[35] Finally, Cpl1 is the lysozyme synthesized by the Cp-1 phage, and it is responsible for bacterial lysis to release the phage progeny.[36] Only the three-dimensional structure of the full parental enzyme is known[37,38] (PDB codes: 1H09 and 1OBA).

In this work we have assessed the affinity of these CBMs for choline and synthetic cell-wall mimics with a variety of biophysical methods. Furthermore, we studied the effects, as possible CBP inhibitors, of externally added CBMs on planktonic cultures of *S. pneumoniae* and finally on the induction of phagocytosis of bacterial cells by mouse peritoneal macrophages. Our results confirm that inhibition of adsorption of CBPs to the cell wall may pave the way for the development of novel, nonlytic antipneumococcal therapies.

RESULTS

Description of Choline-Binding Modules. The C-LytA polypeptide (as coded by the expression plasmid pCE17)[31] contains 5 CBRs (corresponding to CBRs 2−6 of the full-length LytA amidase) plus a hairpin tail (Figure 2A) configuring 4 choline-binding sites of either low or high affinity.[23] On choline binding, dimerization occurs through the

https://dx.doi.org/10.1021/acsinfecdis.9b00344
ACS Infect. Dis. 2020, 6, 954−974

C-terminal hairpin, adopting a "boomerang-like" shape.[33,39] With regard to C-Cpl1, it is made up of 6 CBRs highly similar in sequence to those of LytA[40](Figure 2A) although there are important structural differences among them: C-Cpl1 only contains 2 choline-binding sites, compared to 4 ligands for C-LytA.[33] Moreover, although both proteins acquire a similar "boomerang-like" dimeric shape upon binding of choline, C-Cpl1 dimerizes through the N-terminal part and probably configures an additional choline-binding site at the dimer interface.[41]

The three-dimensional structure of C-CbpD is unknown, although sequence comparison analyses predict the presence of four CBRs, therefore constituting the smallest representative of pneumococcal CBMs described so far.[18,42] Taking advantage of the abundance of similar CBMs with an elucidated tertiary structure, we modeled the structure of C-CbpD with the SwissModel homology procedure (Figure 3).[43] Among all identified targets, the optimal template was the C-terminal part of the choline-binding protein CbpJ.[43] According to the model, the protein acquires the typical β-solenoid disposition of CBRs which is characteristic of the CBP family, with the additional contribution of a C-terminal β-hairpin comprising residues 434−441. Three canonical choline-binding sites are observed in the model, each containing three aromatic residues able to establish direct contacts with the ligand, plus a fourth, inner aromatic side chain stabilizing the cavity through T-shaped $\pi-\pi$ interactions with the central aromatic residue (Figure 3A).[18] Furthermore, a fourth nonstandard binding site involving Tyr 439 in the C-terminal hairpin might also be configured, as described for CbpJ.[44] To assess whether the geometry of these cavities might be suitable for choline binding, we studied their interaction *in silico* with choline molecules by docking procedures using the SwissDock server.[45] As depicted in Figure 3A, the four predicted sites would nicely accommodate the ligands through cation$-\pi$ and van der Waals interactions. Remarkably, the noncanonical site located at the C-terminus would be further stabilized by an additional $\pi-\pi$ contact of Tyr 423 with Tyr 425, also present in the C-terminal tail, leading to a notable network of aromatic residues disposed in a T-shaped stabilizing conformation (Figure 3B).

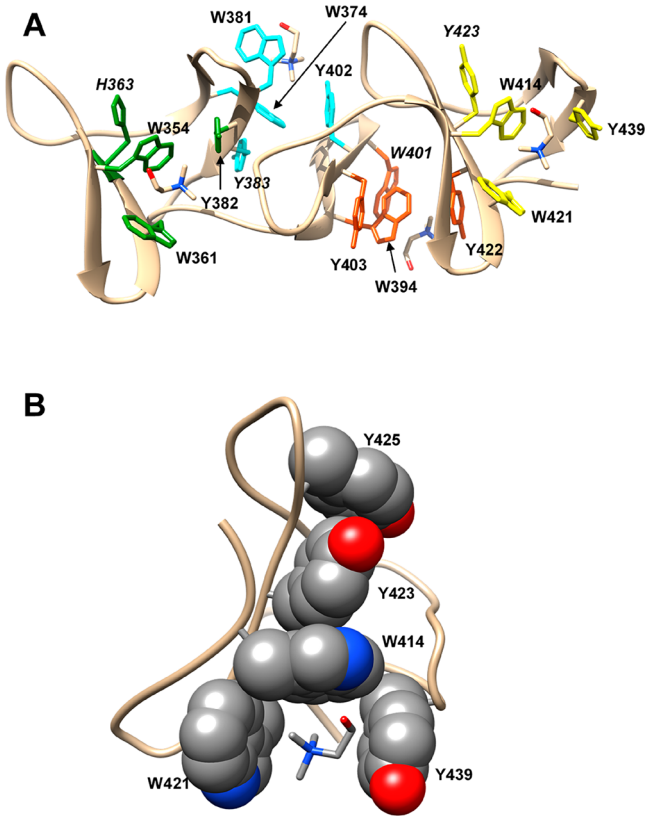

Figure 3. Three-dimensional structural model of C-CbpD generated by the SwissModel and SwissDock servers (see Methods for details). (A) Overall secondary structure representation, showing in stick format the aromatic residues configuring the predicted choline-binding sites (those involved in secondary T-shaped $\pi-\pi$ interactions are labeled in italics). Choline ligands are also shown in stick representation and were generated by docking methods. (B) Closer view of the predicted, nonstandard choline binding site configured by the C-terminal β-hairpin and the following tag. Aromatic residues involved either in direct interaction with the ligand or in the stabilization of the site are shown as van der Waals spheres.

Oligomeric State of CBMs. To carry out the thermodynamic characterization of the binding of choline to CBMs, the oligomerization state of each protein at any ligand concentration should be unequivocally defined. In the case of C-LytA, binding affinity constants have been thoroughly determined[22] (Table 1) and it has been demonstrated that the protein is a dimer above 10 mM choline.[23] The C-Cpl1 protein becomes a dimer at 40 mM choline,[21,41] but there is a lack of information at lower concentrations, and the oligomeric state of C-CbpD has not been studied at all so far. Therefore, to check the oligomeric state of C-Cpl1 and C-CbpD in the absence or presence of 10 mM choline (a concentration often used in our experiments, see below), sedimentation velocity experiments were carried out. Results for C-Cpl1 (Figure 4) in the absence of choline show a single species (>99%) with a sedimentation coefficient of 1.87 S and a frictional ratio (f/f_o) of 1.33, corresponding to the monomer and in agreement with the previously reported results for this protein (1.81 S).[41] In the presence of the ligand, a 2.52 S major species was detected accounting for around 86% of total signal and a frictional ratio (f/f_o) of 1.6, which is compatible with a slightly elongated dimer, in accordance with the previously reported value of 2.58 S registered in 40 mM choline, conditions in which the protein is fully dimeric,[41] whereas a minor percentage (10%) would still be present as a somewhat expanded monomer (1.78 S). The sedimentation velocity profile of C-CbpD (Figure 4) shows in the absence of ligand a major species with sedimentation coefficient of 1.44 S and a fractional ratio (f/f_o) of 1.27, which is compatible with a globular monomer. In the presence of choline the major species shows a nearly identical sedimentation coefficient of 1.46 S, indicating that, contrary to C-LytA and C-Cpl1, the monomeric state of C-CbpD does not change upon ligand binding. All these data concerning the oligomeric state of the CBMs are summarized in Table 1.

Estimation of the Number of Choline Binding Sites in C-Cpl1 and C-CbpD. As mentioned above, the crystal structure of the C-LytA module revealed the existence of 4 bound choline residues per monomer of protein.[33] On the other hand, no structure of the isolated C-Cpl1 protein is available, and only the crystal structure of the full Cpl-1 monomer has been reported, revealing two choline molecules bound. However, it should be pointed out that such structure was elucidated upon soaking the ligand-free protein crystals in

https://dx.doi.org/10.1021/acsinfecdis.9b00344
ACS Infect. Dis. 2020, 6, 954−974

Table 1

	Oligomeric state				K_d (μM)		
	No choline	+10 mM choline	Number of CBRs[a]	Number of binding sites[a]	Choline	DEAE-MNPs	SPR DEAPA chips
C-Cpl1	Monomer	Dimer	12 (6 + 6)[40]	5 (2 + 2+1)	670 ± 50	16 ± 4	9 ± 1
C-CbpD	Monomer	Monomer	4[42]	4	300 ± 10	23 ± 6	N.D.[b]
C-LytA	Monomer	Dimer	10[31] (5 + 5)	8[33] (4 + 4)	100 and 5300[c22]	54 ± 9	0.19 ± 0.01 (25% signal)[c] 14 ± 7 (75% signal)[c]
LZ-C-LytA	N.D.	Trimer/dimer	15/10 ([5]+5 + 5)	12/8 ([4]+4 + 4)[d]	N.D.[b]	N.D.[b]	1.8 ± 0.3

[a]Number of CBRs or sites of the choline-bound species in its corresponding oligomeric state. Parentheses make reference to each of the monomers. [b]N.D.: Not determined. [c]High- and low-affinity sites, respectively. [d]Theoretical estimation.

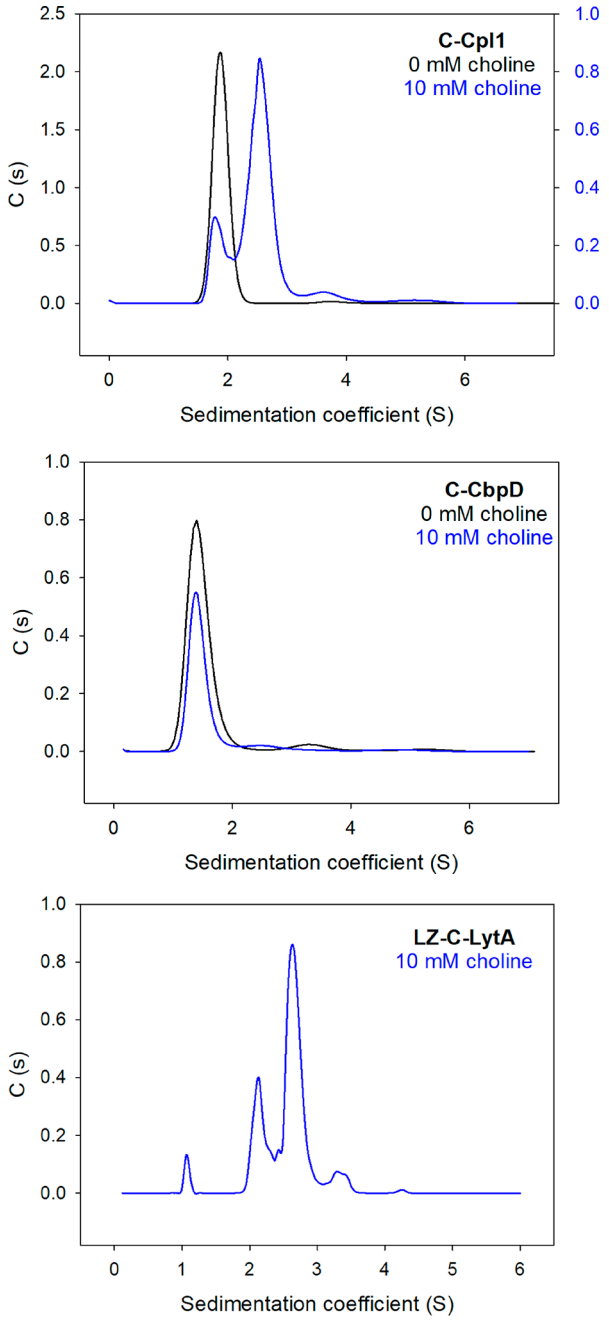

Figure 4. Sedimentation velocity experiments of CBMs in the absence or presence of choline.

a choline solution,[37] so that the dimerization process could not take place under such circumstances. Moreover, the binding capacity of the isolated C-Cpl1 module, in the absence of the catalytic domain, might be different from that within the parental enzyme. Therefore, we decided to experimentally determine the number of bound ligand molecules for both CBMs by van't Hoff thermal analysis.[46,47] The thermal stability was assessed by monitoring the circular dichroism (CD) signal in the far-UV region (224 nm) at increasing choline concentrations. This technique reports on both the secondary and tertiary structures of CBMs due to the extensive overlap of contributions arising both from the peptide bonds and from the aromatic side chains,[22,31] which is reflected in the unusual positive bands in the 220−240 nm region (Figures 5A and B), so that this parameter constitutes a suitable probe for the overall structure of these proteins. The ligand induces an increase in the ellipticity of both proteins, which is more evident for C-Cpl1 (Figures 5A and B), and confers stability to both proteins by inducing an increase in its denaturation temperature midpoint (T_m) (Figures 5C−D). Although the proteins were not able to renature after cooling down the sample (data not shown), the thermal transitions were fitted to the Gibbs−Helmholtz thermodynamic equation (eq 1), as we determined that the thermal scans were independent of the heating rate (20−50 °C h^{-1}), so any irreversible step in the denaturation process is slower than the equilibrium denaturation event.[24,48]

The use of the Gibbs−Helmholtz equation requires the previous knowledge, or estimation, of the difference in heat capacity between the folded and the unfolded states (ΔC_p). Several theoretical procedures were followed (see Methods), and the results are displayed in Table S1. One method is based only on the number of protein residues[49] (eq 2). Nevertheless, we also made use of the three-dimensional structure of the full-length parental Cpl1,[37] from which the structure of the isolated C-Cpl1 module can be deduced to be very similar, as demonstrated by SAXS experiments.[41] Regarding C-CbpD, we made use of the homology model described above. With these structures, we employed the theoretical approaches described by Myers et al.[50] and Spolar et al.[51] (eqs 3 and 4, respectively), which make use of the differences in accessible surface area between the folded and the unfolded states. Despite the theoretical differences among the three approaches, the results of the calculations were remarkably similar (Table S1), so that an average value of ΔC_p was finally estimated for C-Cpl1 (2.0 cal mol^{-1} K^{-1}) and for C-CbpD (1.2 cal mol^{-1} K^{-1}).

The vant Hoff analysis of C-Cpl1 thermal unfolding scans (eq 5) is shown in Figure 5E, yielding a value of n = 5.0 sites per cooperative denaturation unit. Since, at the concentrations tested, C-Cpl1 is a dimer (Figure 4), the results are then compatible with the presence of 2 bound ligands per monomer

https://dx.doi.org/10.1021/acsinfecdis.9b00344
ACS Infect. Dis. 2020, 6, 954−974

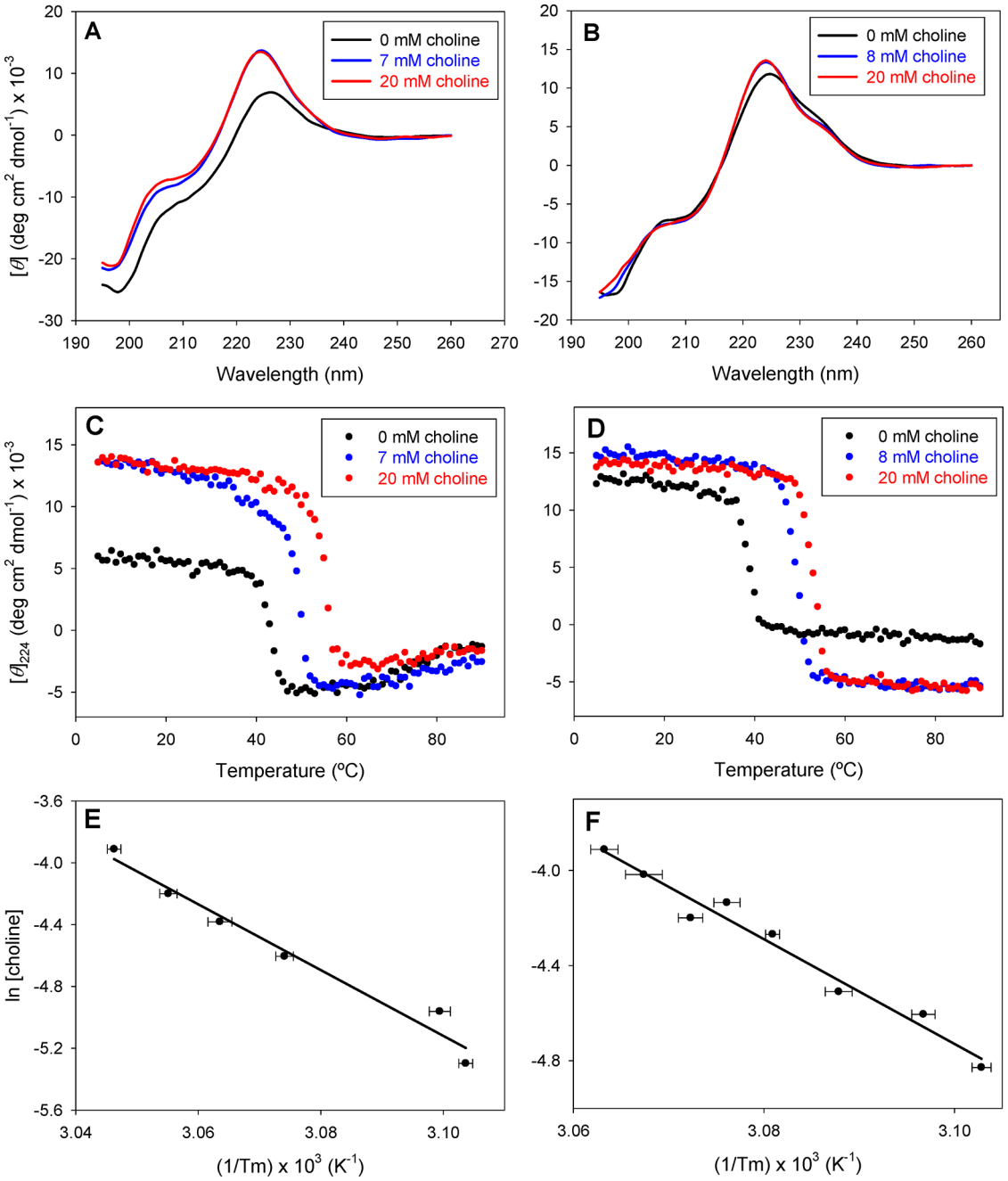

Figure 5. Circular dichroism studies on C-Cpl1 and C-CbpD. Far-UV CD spectra of C-Cpl1 (A) and C-CbpD (B) in the absence or presence of choline; CD-monitored thermal stability of C-Cpl1 (C) and C-CbpD (D) in the absence or presence of choline; (E) van't Hoff plot of C-Cpl1 thermal denaturation; the slope of the fit to eq 5 was −21000 ± 2000 K and the mean unfolding enthalpy was 206 ± 20 kcal mol^{-1}, leading to n = 5.0 sites per denaturation unit (dimer); (F) van't Hoff plot of C-CbpD thermal denaturation; the slope of the fit to eq 5 was −22000 ± 1500 K and the mean unfolding enthalpy was 170 ± 20 kcal mol^{-1}, leading to n = 3.9 sites per denaturation unit (monomer). Data shown in panels E and F are the average of at least 3 scans.

plus an additional one probably located at the dimerization interface and configured by residues W210, F218, and Y238 of each monomer, as previously suggested.[41] Regarding C-CbpD, the van't Hoff analysis (Figure 5F) yielded, in this case, a value of n = 3.9 ligand molecules per monomer, in agreement with the 4 predicted binding sites considered in the structural model of the protein (3 standard sites plus a noncanonical additional one, Figure 3). It should be pointed out that nonspecific effects of choline chloride on protein stability due to the increase in ionic strength should be ruled out, at least at the concentrations used (0−20 mM), since temperature scans of both C-Cpl1 and C-CbpD either in the presence or the absence of 20 mM NaCl yielded the same thermodynamical results (data not shown).

Affinity Binding of Soluble Choline to CBMs. Choline binding affinity for C-LytA protein has been previously determined, unraveling the existence of low- and high-affinity binding sites (Table 1).[22] To estimate the binding constants for C-Cpl1 and C-CbpD, equilibrium titrations were carried out by following the change in the intrinsic fluorescence spectra upon addition of the ligand. In both cases the addition of choline induces a decrease in the signal concomitantly with

https://dx.doi.org/10.1021/acsinfecdis.9b00344
ACS Infect. Dis. 2020, 6, 954−974

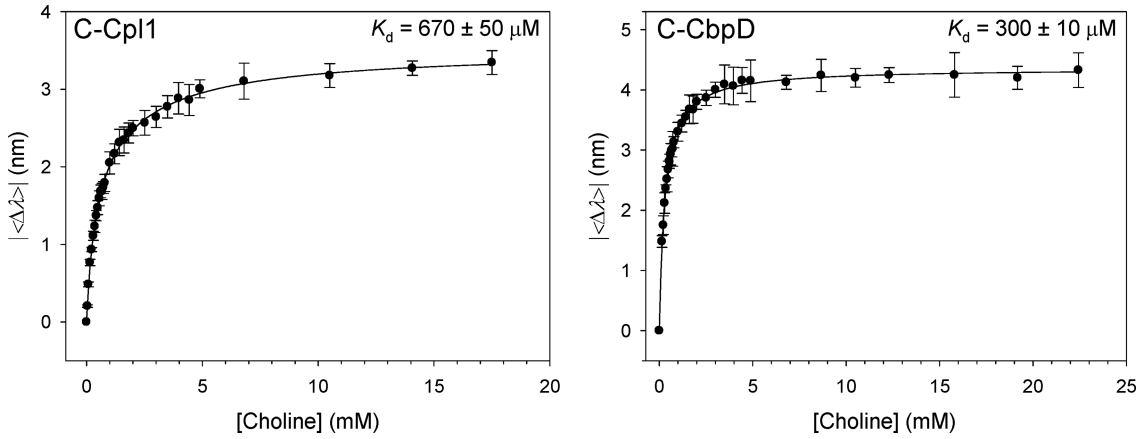

Figure 6. Titration curves of C-Cpl1 and C-CbpD with choline, monitored by intrinsic fluorescence (absolute value of changes in average emission intensity). The average values of triplicates are shown.

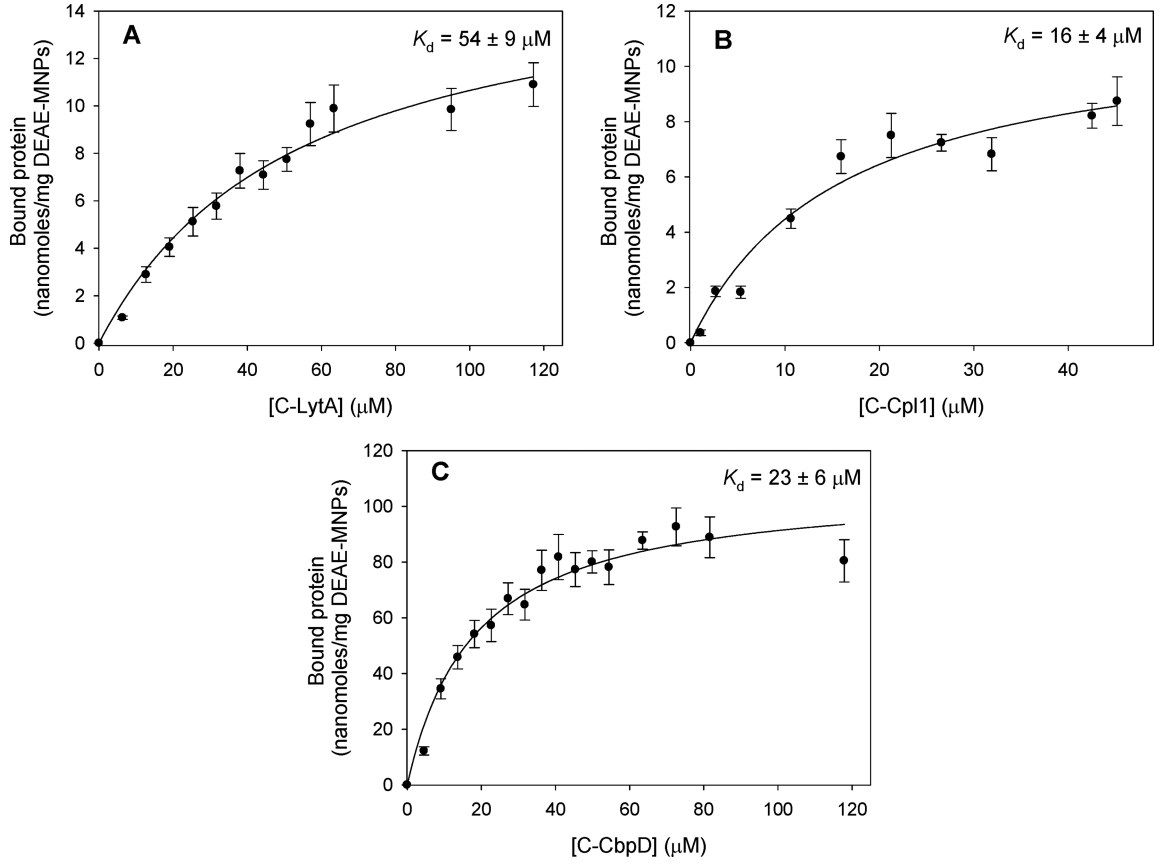

Figure 7. Langmuir binding isotherms of CBMs to DEAE-MNPs. Experiments were performed in triplicate.

an evident blue-shift (Figure S1), indicating both an enhanced quenching and a decrease in the polarity of the environment surrounding the tryptophan residues. Spectra of the proteins recorded in the presence of 20 mM NaCl showed no significant (C-Cpl1) or very slight (C-CbpD) differences in the fluorescence intensity, as well as negligible changes in the wavelength of the peak maximum (Figure S1) therefore discarding important, nonspecific ionic strength effects. Both C-Cpl1 and C-CbpD display a well-defined hyperbolic binding curve when monitoring the absolute value of the changes in average emission intensities ($|\langle\lambda\rangle|$) (eq 6, Figure 6). Dissociation constants (K_d) were calculated assuming that all binding sites had similar affinity, as previously described for Cpl-1.[21] Analysis of titration curves (Figure 6) considered the binding of 5 molecules, coupled with dimerization, to C-Cpl1, assuming a negligible presence of protein dimers in the absence of choline (eq 7) or the independent binding of 4 molecules to C-CbpD monomers (eq 8).

The calculated constants (K_d = 0.67 ± 0.05 mM for C-Cpl1 and 0.30 ± 0.01 mM for C-CbpD, Table 1) are intermediate between the high- and low-affinity sites in C-LytA (0.1 mM and 5.3 mM, respectively)[22] and indicate a higher affinity by C-CbpD for the ligand than C-Cpl1. It is noteworthy that the K_d value for C-Cpl1 (0.67 mM) is lower than that reported for the full-length parental Cpl1 enzyme derived from CD-monitored (3.6 mM) and isothermal titration calorimetry titrations (1.9

https://dx.doi.org/10.1021/acsinfecdis.9b00344
ACS Infect. Dis. 2020, 6, 954−974

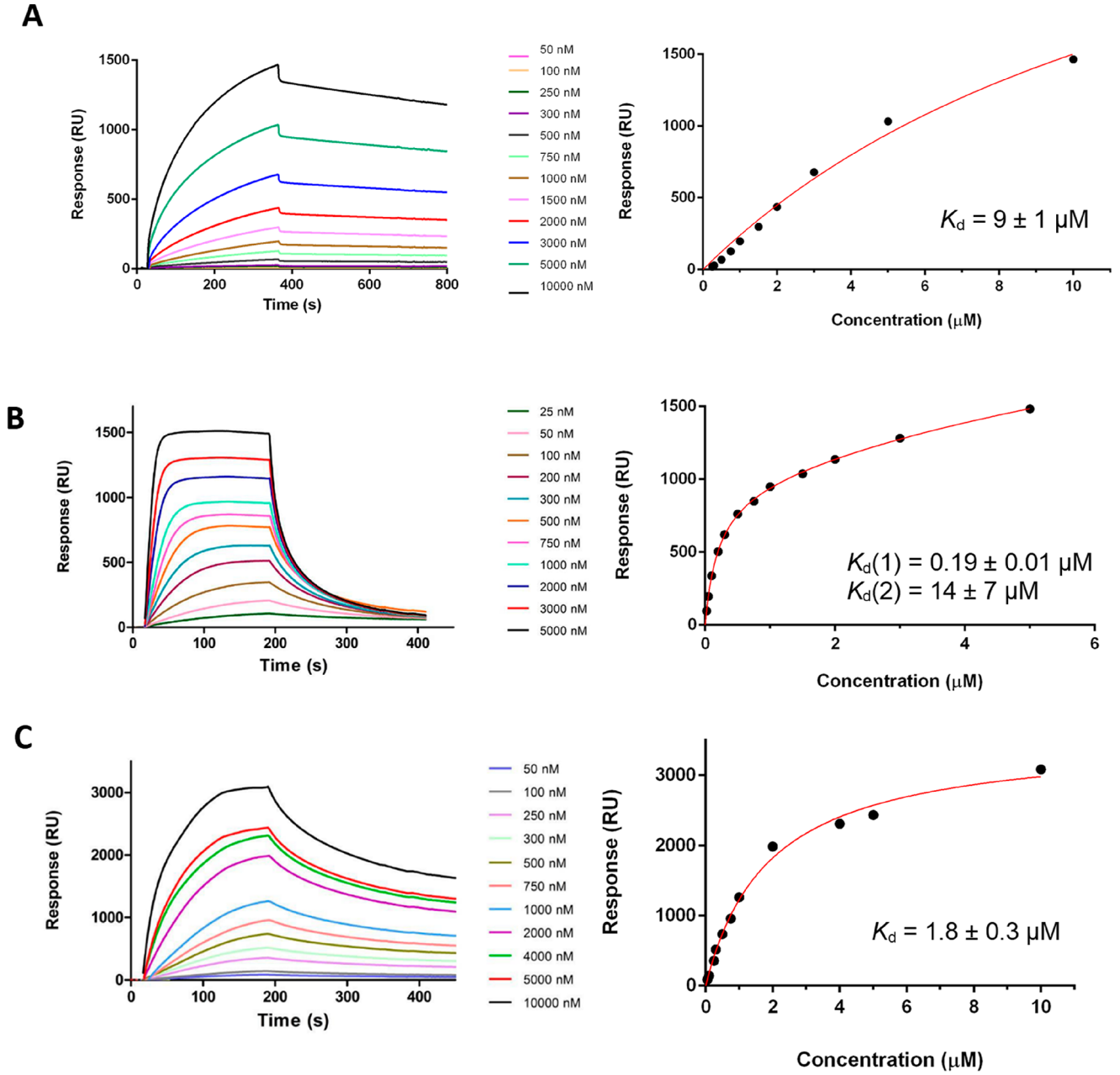

Figure 8. Surface plasmon resonance (SPR) analysis of the interaction of CBMs with DEAPA-coated chips. Left: SPR sensorgrams. Right: Binding plots derived from SPR sensorgrams used to calculate the affinity constants. (A) C-Cpl1; (B) C-LytA; (C) LZ-C-LytA. Experiments were carried out in duplicate, but only a sample is shown in the figure.

mM).[21] These discrepancies might arise from the previous consideration based on the crystal structure,[37] of 4 binding sites instead of the 5 that we postulate here, and/or from the strong interaction present, in the parental enzyme, between catalytic and choline-binding modules[37] that could somehow obstruct the binding of the ligand and, consequently, the dimerization of the protein. In fact, differential scanning calorimetry (DSC) studies previously carried out with both Cpl-1 and C-Cpl1 proteins showed that, in the presence of 10 mM of choline, the differences between the calorimetric and the van't Hoff denaturation enthalpies could be explained if the C-Cpl1 module was present as a dimer whereas only 30% of the parental protein acquired a dimeric conformation in these conditions.[24]

In any case, the estimated dissociation constants are of high magnitude (millimolar range), confirming that the affinity of CBMs for free choline is very low in general terms. Therefore, to explain the high affinity shown by CBMs for the cell wall, synthetic systems should be used that take into account the multivalency effects arising from the multiple disposition of choline receptor molecules on a supramolecular, polydentate structure.

Binding of CBMs to Solid-State Cell-Wall Mimics. To avoid any discrepancies due to the lack of homogeneity of different cell wall preparations that would hamper a suitable comparative binding analysis using this natural substrate, and taking advantage of the wide range of choline analogs able to interact with CBMs,[52,53] we made use of two types of cell-wall mimics functionalized with multiple copies of a choline

https://dx.doi.org/10.1021/acsinfecdis.9b00344
ACS Infect. Dis. 2020, 6, 954−974

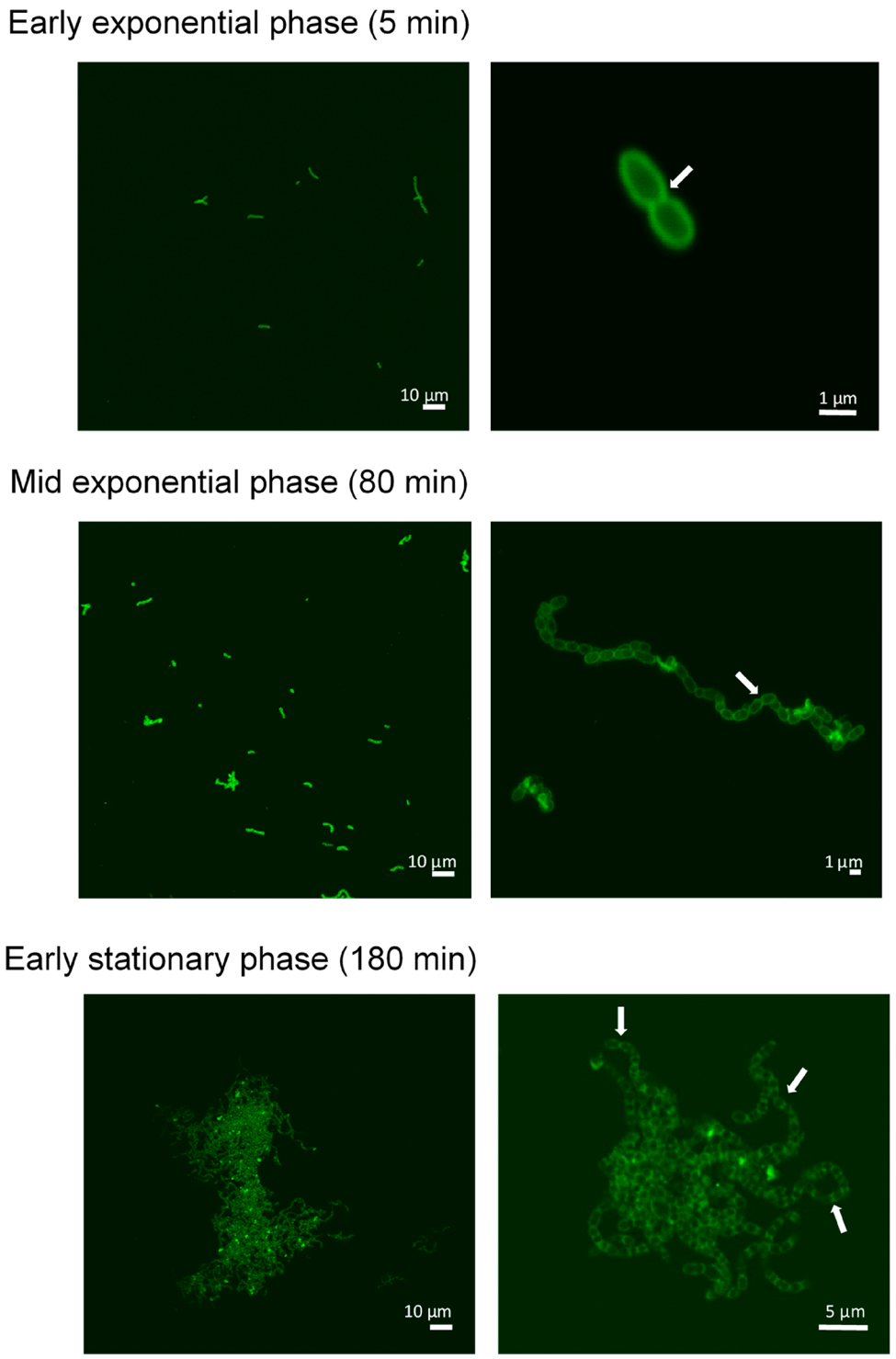

Figure 9. Fluorescence microscopy micrographs of *S. pneumoniae* R6CIB17 cultured in the presence of GFP-C-LytA (1 μM). The time after protein addition at an OD_{550} of 0.1 is indicated. Arrows indicate the position of bacterial septa.

analogue: (i) magnetic nanoparticles (200 nm) functionalized with 2-diethylaminoethyl-starch groups (DEAE-MNPs) and (ii) surface plasmon resonance (SPR) chips derivatized with *N,N*-diethyl-1,3-diaminopropane (DEAPA). It should be recalled that DEAE is an usual compound in the affinity chromatography resins employed to purify CBPs[52,53] and that the specific binding of CBPs to the DEAE-MNPs has already been previously reported in our laboratory.[54] Binding of the three CBMs to the DEAE-MNPs was subjected to Langmuir analysis (eq 9, Figure 7). The calculated apparent K_d values are shown in Table 1. In the case of C-LytA protein, and despite that protein harbors two types of binding sites for choline,[22] a single apparent dissociation constant could only be discerned (54 ± 9 μM), with other alternative fittings being unsuccessful (data not shown). Regarding C-Cpl1 and C-CbpD proteins, the obtained K_d's were comparable (16 ± 4 and 23 ± 6 μM, respectively) and reflect a higher affinity for the solid substrate

https://dx.doi.org/10.1021/acsinfecdis.9b00344
ACS Infect. Dis. 2020, 6, 954−974

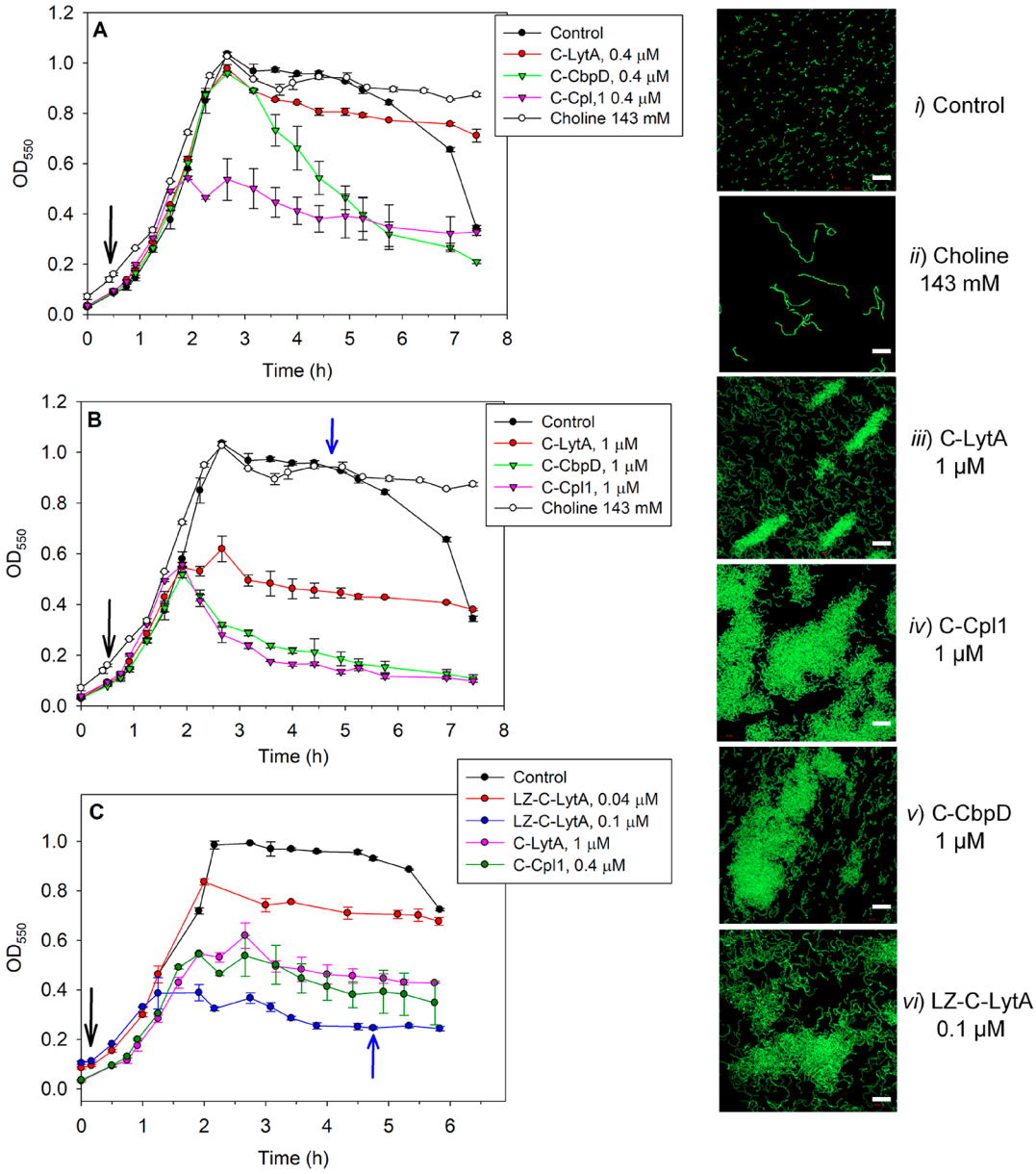

Figure 10. Effect of addition of CBMs to pneumococcal planktonic cultures. Left: growth curves. Black arrows indicate time of CBM addition to the medium, and blue arrows indicate time of sample removal for microscopy. Experiments were performed in duplicate. Right, confocal fluorescence microscopy micrographs (i–vi) of samples taken from the bottom of the tube in the stationary phase of the culture. Cells were stained with the *BacLight* kit. Bars indicate 10 μm.

than C-LytA even though they possess fewer choline-binding sites (Table 1, Figure 2).

The affinity analysis and binding kinetics of CBMs were also determined by SPR. The purified proteins were applied to sensor chips coated with DEAPA. Representative sensorgrams for C-Cpl1 and C-LytA are presented in Figure 8. The C-CbpD protein could not be used for SPR experiments due to a nonhomogeneous behavior at any of the densities used, probably due to protein aggregation on the surface (data not shown). The binding of C-LytA to the DEAPA surface (Figure 8B) displayed similar characteristics than those to soluble choline, as it could only be analyzed in terms of a two-site affinity model, with 75% of the signal corresponding to the low affinity sites (K_d = 14 ± 7 μM) and 25% of the signal representing the high affinity sites (K_d = 0.19 ± 0.01 μM). The binding curve of C-Cpl1 (Figure 8A) was, conversely, best fitted to a single-site affinity model (K_d = 9 ± 1 μM), again representing an intermediate value between the two types of C-LytA sites (Table 1). The dissociation constants obtained from the two experiments employing a polydentate, solid substrate representing binding affinities 20–500-fold higher than those for the free ligand (Table 1), highlighting appreciable multivalent effects that may be extrapolated to the bacterial cell wall.

Effect of Exogenously Added CBMs to Pneumococcal Planktonic Cultures. The results shown so far indicate that CBMs are able to efficiently interact with choline analogs contained on the surface of insoluble, multivalent substrates. Our next step was testing whether CBMs added to a pneumococcal culture could compete with the bacterial CBPs for binding to the choline in the cell wall, therefore inhibiting these proteins. In support for this hypothesis, it

https://dx.doi.org/10.1021/acsinfecdis.9b00344
ACS Infect. Dis. 2020, 6, 954–974

should be mentioned that we had previously described that the C-Cpl1 or C-LytA modules inhibit the activity of the parental Cpl1 and LytA hydrolases in cell-wall hydrolysis experiments *in vitro*.[31] If successful, effects such as prevention of autolysis or inhibition of separation of daughter cells upon division might be expected, leading to the formation of long chains, as it has been long observed upon addition of an excess of choline to the medium.[20] To facilitate the observations, the experiments were carried out with the R6CIB17 strain, a derivative of the commonly used noncapsulated R6 laboratory strain that was identified in our group and that does not flocculate in liquid medium (see Methods). A detailed description of this strain will be published elsewhere. First, we added to a bacterial culture a hybrid protein (GFP-C-LytA) in which the green fluorescent protein (GFP) is fused to the C-LytA module.[55] The protein was added in early exponential phase ($OD_{550} \approx 0.1$), and samples taken at different times were observed by fluorescence microscopy. As depicted in Figure 9, as early as 5 min after addition, the GFP-C-LytA protein was evenly distributed on the bacterial surface. As the growth proceeded, long chains were visible and, at the start of the stationary phase, appreciable cell clumps were detected while most of the fluorescence was kept in the bacterial septa (Figure 9). In fact, the septum has been described to be the destination of intracellularly expressed, full-length LytA autolysin,[56] confirming the preference of the C-LytA moiety to the equatorial region in the cell in the later stages of growth.

The pneumococcal strain R6CIB17 was cultured in test tubes without shaking or turning over prior to measuring the optical density (OD_{550}). In these conditions, cells acquire the usual diplococcal shape or form very short chains (Figure 10, panel i), and finally undergo autolysis at the end of the stationary phase, detected as a decrease in optical density in control experiments (Figure 10A−C). Addition of choline, on the other hand, induces the formation of long chains (Figure 10, panel ii) that do not autolyse nor flocculate (Figure 10A−B). To test the effect of CBMs, these proteins were added to the culture in the early exponential growth phase ($OD_{550} \approx 0.1$) to a final concentration of 40 nM, 400 nM, and 1 μM. No effect was shown by any of the CBMs tested at 40 nM (data not shown). However, upon addition of 400 nM C-Cpl1, visible aggregates were soon observed and subsequently deposited in the bottom of the tube, leading to a decrease in the OD_{550} of the supernatant (Figure 10A) (Samples of cell clumps observed upon addition of 1 μM CBMs are shown in Figure 10, panels iii−vi). A similar result was observed with C-CbpD, although in this case visible aggregation was only detected at the end of the exponential phase (Figure 10A). Regarding C-LytA, this protein did not lead to flocculation at this concentration (400 nM), although a clear prevention of autolysis at the end of the stationary phase was evident (Figure 10A). On the other hand, when the concentration of the CBMs was increased to 1 μM, a much more pronounced effect was achieved, leading to cell deposition even in the case of C-LytA (Figures 10 and S2). As mentioned above, no cell aggregation was observed when choline was added to the culture (Figures 10A−B and panel ii), suggesting additional mechanisms of action exerted by the CBM polypeptides compared to the aminoalcohol.

Samples of cultures containing 1 μM of each corresponding CBM were taken in the stationary phase, both from the upper part and the bottom of the culture tube, and characterized by confocal microscopy upon staining with the *LIVE/Dead BacLight* bacterial viability kit. The same sample was used to calculate the number of viable cells. Samples of the upper part of the tube were almost devoid of cells (data not shown), whereas those from the bottom contained a vast majority of green-stained cell chains of smaller length than those induced by choline but, above all, accumulated as cell aggregates which were of bigger size in the case of C-Cpl1 and C-CbpD (Figure 10). Besides, viability tests confirmed that the addition of CBMs to the bacterial culture did not induce cell death (data not shown), in agreement with the observation that the vast majority of cells were green-labeled in all cases when stained with the *BacLight* kit, demonstrating that the bacterial membrane was not compromised and therefore ruling out any lytic effect induced by CBMs (Figure 10). These results suggest that the bacterial aggregation could arise from the formation of cell chains as a consequence of bacterial host CBP inhibition. However, the fact that a chaining phenotype is also achieved upon CBP inhibition by addition of choline, but in the latter case the cells are kept in suspension, suggests that added CBMs must participate in additional cell−cell interactions that lead to aggregation. Moreover, those CBMs displaying a higher affinity to DEAE-containing supramolecular substrates (C-Cpl1 and C-CbpD, Table 1) were also the most effective in inducing the flocculation effects.

Enhancing the CBM Flocculating Effect by Protein Engineering. As described above, the interaction between CBMs and the pneumococcal surface (or mimics thereof) displays the classical multivalency features arising from two polydentate entities: a protein with several choline-binding sites and a substrate with multiple choline/choline analogs. Our results also show that there seems to be no direct correlation between the number of choline-binding sites and affinity for the substrate (Table 1). Nevertheless, we decided to study the effect of increasing the number of ligand-binding[27] sites per molecule but in a branched, rather than linear, disposition, based on dendrimeric structures that have been previously used by our group to enhance the effect of choline and choline analogs on pneumococcal cultures.[26,27,57] To do so, we designed an oligomeric derivative of the C-LytA module (LZ-C-LytA), containing the leucine zipper sequence (LZ) of the PhaF protein from *Pseudomonas putida* KT2440, which has been described as a protein oligomerization motif.[58,59] The LZ sequence was fused to the N-terminus of C-LytA and separated by a linker to prevent possible steric hindrances that would hamper choline-induced oligomerization (Figure S3). The reason to choose C-LytA was to test the real possibilities of our approach to improve the properties of the CBM with the smallest affinity for DEAE-containing substrates and the lowest effectiveness on the pneumococcal cultures.

The LZ-C-LytA polypeptide was overexpressed and purified by affinity chromatography in DEAE-cellulose as described in the Methods. To determine the oligomerization state of the LZ-C-LytA, a sedimentation velocity experiment was carried out in the presence of 10 mM of choline. The experiment could not be performed in the absence of choline due to the aggregation of the sample in the ultracentrifugation conditions. The results shown in Figure 4 and Table S2 show that in the presence of choline the protein exists as a mixture of species: a major one of 2.69 S (64%), an additional one of 2.20 S (27%), and two minor species of 1.09 S (3%) and 3.36 S (6%). The presence of choline complicates the analysis to determine the nature of the LZ-C-LytA complexes, since, in these conditions, the protein could oligomerize via the C-terminal of the C-LytA

https://dx.doi.org/10.1021/acsinfecdis.9b00344
ACS Infect. Dis. 2020, 6, 954−974

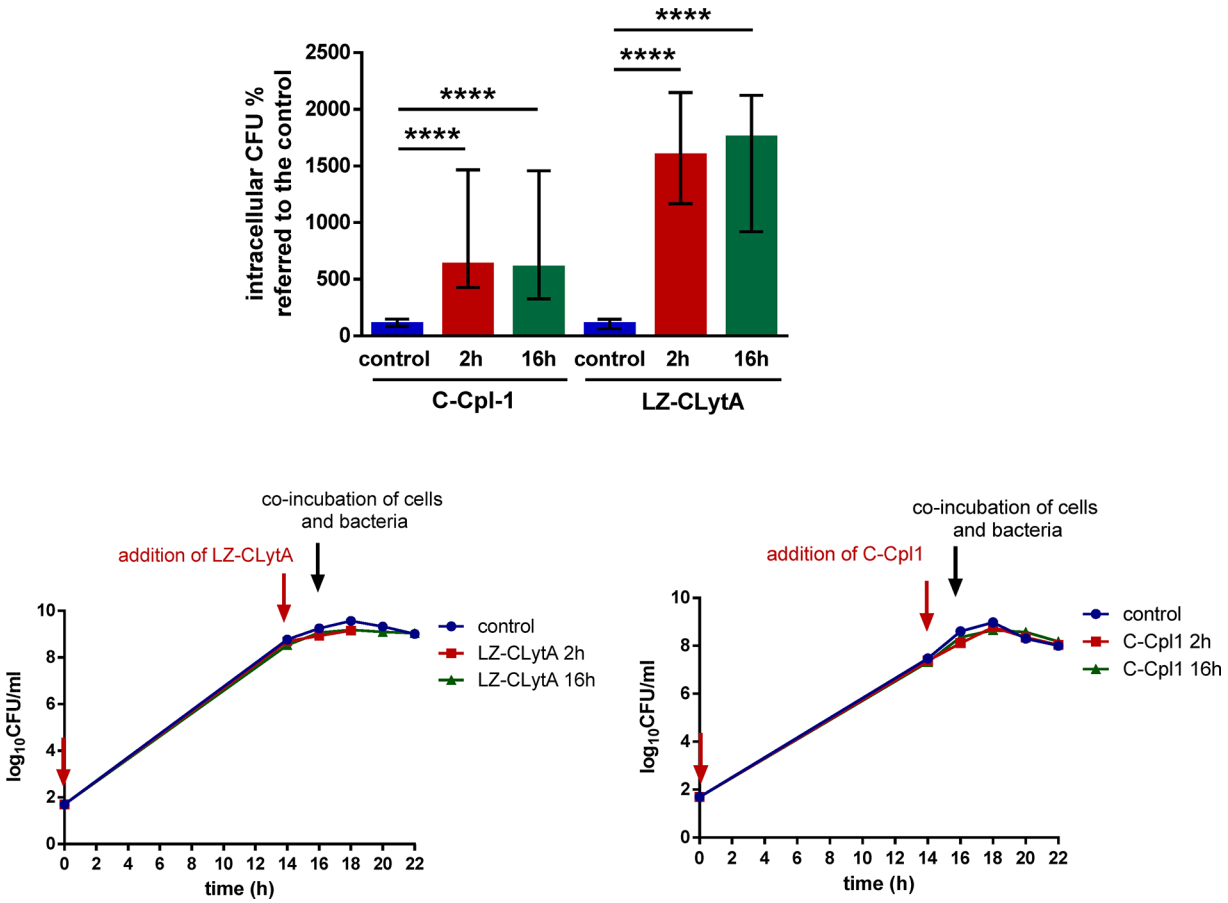

Figure 11. Pretreatment of pneumococci with choline-binding modules (CBM) increases their phagocytosis by macrophages. Comparison of the numbers of intracellular colony forming units (CFU) after 2 h (red bars) and 16 h (green bars) of pretreatment of a R6 pneumococcal culture with either 1 μM C-CpI1 (cells from 7 animals; 20−21 measurements/group) or 1 μM LZ-C-LytA (cells from 5 animals; 19−20 measurements/group). The numbers of bacteria phagocytosed after CBM pretreatment within 1 h were expressed in % of the numbers of untreated bacteria phagocytosed in the same time interval. Data are expressed as medians (25th percentile/75th percentile). Kruskal−Wallis test followed by Dunn's multiple comparison test was used to compare data (****, $p < 0.0001$).

moiety and/or via the LZ sequence. In an attempt to assign each sedimentation signal to the possible oligomeric complexes, we generated *in silico* the three-dimensional structures of all possible oligomers (see Methods for details) (Figure S3). Briefly, a model of the LZ sequence[58] was linked to C-LytA to generate the core monomer. Next, the dimer involving interactions between C-LytA C-terminal hairpins (CT2 variant) was generated with a Swiss-PDB viewer by homology modeling based on the crystal structure of the C-LytA dimer,[33] while the dimer involving LZ-LZ interaction (LZ2 variant) was generated using the M-ZDOCK server.[60] On the other hand, among the variety of possible higher-order oligomers (trimers and tetramers) we decided to discard those models containing mixed LZ-LZ and C-LytA-C-LytA interactions. The reason is that those models would contain unpaired oligomerization motifs that should lead to further polymerization, in contrast with the analytical centrifugation results (Figure 4). As a consequence, only LZ-based oligomers were considered (LZ3 and LZ4, Figure S3). Next, the hydrodynamic properties of the structures were estimated using the HydroPRO utilities.[61] Table S2 displays a comparison among the experimental and predicted values of the sedimentation coefficients. The major peak in the sedimentation profile (2.69 S) is compatible with a trimer, whereas the 2.20 S species could represent a dimer, and the minor peaks might correspond to monomers and tetramers. The theoretical hydrodynamic predictions of the *in silico* models (Table S2) are, within the limits of this approach, reasonably compatible with the experimental sedimentation results, prompting us to predict the predominant presence of the LZ-oligomerized species depicted in Figure S3.

Next, we determined the affinity of the LZ-C-LytA oligomers to DEAE-functionalized surfaces. The binding to DEAE-MNPs could not be carried out due to protein aggregation at the concentrations needed. However, SPR experiments, which make use of a much lower concentration, yielded the sensorgram shown in Figure 8C. Unlike C-LytA (Figure 8B), data for LZ-C-LytA could only be properly fitted assuming one type of binding sites (K_d = 1.8 ± 0.3 μM, Table 1). The high-affinity sites of C-LytA are involved in protein dimerization through the C-terminal hairpins.[23,34,62] However, this interaction might be hampered by the alternative LZ-LZ-mediated oligomerization (Figure S3), which could leave the C-terminal hairpins without the possibility of interaction, mostly due to steric hindrance reasons, and with the result of the conversion of all binding sites to the "low-affinity" kind. In support of this, it has been previously described that LytA variants which had their C-terminal tags truncated or deleted do not display high-affinity binding sites anymore.[62,63] With this hypothesis in mind, upon comparison with the affinity of

https://dx.doi.org/10.1021/acsinfecdis.9b00344
ACS Infect. Dis. 2020, 6, 954−974

the major fraction of C-LytA sites for SPR chips (75% of population, K_d = 14 μM), the incorporation of the LZ motif would result in an 8-fold increase on the affinity. This would indicate that the oligomerization of a protein (C-LytA) with moderate binding capacity leads to a significant increment in the affinity for its ligand. In fact, LZ-C-LytA turned out to be the best binder among those CBMs tested by SPR (Table 1).

To assess whether the enhancement in binding properties shown by LZ-C-LytA had a reflection on the bacterial culture assays, the protein was added to a planktonic culture of R6CIB17 at early exponential phase (Figure 10C). A slight effect on the OD_{550} was observed at a concentration as low as 40 nM of added LZ-C-LytA, similar to that obtained at 400 nM of C-LytA (Figure 10A). Nevertheless, results are more evident at 100 nM concentration which caused eye-visible bacterial aggregation and a OD decrease comparable to that obtained using higher concentrations of C-Cpl1 (400 nM) and C-LytA (1 μM) (Figure 10C). Moreover, the confocal images of *BacLight*-stained samples taken from the bottom of the tube containing 0.1 μM of LZ-C-LytA (stationary phase) showed the accumulation of long, green-stained cell chains (Figure 10, panel vi), whereas the number of viable cells remained unchanged (data not shown). These results indicate that the multivalent presentation of CBMs in a branched disposition exponentially augments the binding affinity to the choline in the cell wall and concomitantly reduces the necessary concentrations to induce bacterial aggregation.

Phagocytosis of *S. pneumoniae* Previously Treated with CBMs by Peritoneal Macrophages. Our results suggest that the incubation of pneumococcal cultures with a CBM does not arrest the cell division or decrease viability but induces the cell aggregation and/or establishment of long chains, and these effects could in fact facilitate bacterial phagocytosis by the host macrophages, as we have previously demonstrated for cultures treated with choline dendrimers.[27] To test this hypothesis, we compared the number of intracellular colony forming units (CFU) after 2 and 16 h of pretreatment of a R6 pneumococcal culture either with C-Cpl1 or LZ-C-LytA at a final concentration of 1 μM with the number of bacteria phagocytosed by macrophages without CBM pretreatment (please note that here we used the R6 naturally flocculating strain and not our R6CIB17 derivative used in the planktonic assays). To account for intraday variation of the assay, the number of bacteria phagocytosed after CBM pretreatment within 1 h was expressed in % of the number of bacteria phagocytosed in the same time interval without pretreatment (Figure 11). Compared to the control samples without CBM added, the phagocytosis of bacteria substantially increased when the culture was previously treated with the CBMs, irrespective of the coincubation time (Figure 11). Remarkably, the percentage of intracellular CFU was nearly 3 times higher with LZ-C-LytA compared to C-Cpl1, mirroring their binding affinities to SPR DEAPA chips *in vitro* (5-fold higher affinity for the former protein, Table 1 and Figure 8) and the agglutination effects in planktonic cultures (Figure 10), where a 0.1 μM concentration of LZ-C-LytA produced approximately the same aggregation effect (as measured by optical density) as a 4−5-fold higher concentration of C-Cpl1 (0.4 μM). In any case, when carrying out these comparisons, it should be taken into account that the aspects of the aggregates produced by the two proteins are somewhat different, with longer chains in the case of LZ-C-LytA (Figure 10), and this may have some influence both on the sedimentation properties of the cell aggregates in the liquid cultures and, above all, on a highly complex phenomenon such as phagocytosis.

DISCUSSION

The choline-binding protein system of *S. pneumoniae* constitutes a paradigmatic example of modular evolution[40,64] that is essential for pneumococcal viability and virulence.[18] This reason, together with the common mechanism shared by all members of the family to recognize the choline residues contained in the cell-wall, shows clues for the development of compounds that might simultaneously inhibit or interfere with their activity and that could represent a novel set of antimicrobials to tackle current antimicrobial resistance. Since the use of lytic compounds may not be devoid of harmful consequences due the uncontrolled release of virulence factors and toxic compounds from the bacterial cytoplasm,[28,29] we decided to investigate the effect of exogenous CBMs as surface choline blockers, with the aim of generating cell chains and aggregates that reduce bacterial dissemination, promote host phagocytosis, and, eventually, favor complement deposition as previously described[32] (Figure 1).

Initially we carried out a detailed structural analysis of three representative CBMs, namely C-LytA, C-Cpl1, and C-CbpD, differing in size, number of CBRs, and binding sites, as well as in oligomeric state (Figures 2−5, Figure S1 and Table 1). Their affinity for free choline and polydentate supramolecular substrates was also assessed (Figures 6−8 and Table 1). Then, taking advantage of their ability to bind to the cell wall mimics, they were assayed on pneumococcal planktonic cultures (Figures 9 and 10 and S2) with the aim of saturating the choline residues in the teichoic and lipoteichoic acids and make them unavailable for the full-length CBPs. Remarkably, in addition to the formation of long chains as a consequence of inhibiting those CBP hydrolases involved in separation of daughter cells upon division (similar to the addition of choline), the three tested CBMs also induced, to a variable extent, the aggregation of pneumococcal cells, even leading to visible clumps (Figures 9 and 10 and S2). A rationally engineered form of a CBM (Figure S3) successfully made use of multivalency principles to enhance its substrate recognition and aggregating activity (Figures 8 and 10, Table 1). Finally, these observations were exploited to check the ability of the CBMs to augment bacterial phagocytosis by mouse peritoneal macrophages (Figure 11). All these results together point to CBMs as a novel streamlined alternative of nonlytic antipneumococcal compounds aimed to facilitate the natural defense mechanisms of the infected host.

Many intriguing questions have arisen from the pneumococcal CBP system from the structural point of view given the wide variety in geometries and number and disposition of CBRs displayed by CBMs.[18] For instance, is the affinity for choline directly related to the number of choline-binding sites? Previous studies suggested that this is not necessarily the case, at least regarding free choline. The affinity for free choline in solution has been shown to be similar both for LytC and Cpl1,[21] but the former contains 7 binding sites per monomer[38] while the latter possesses 5 sites per dimer, as we show here. In the same line, full-length LytA contains 10 canonical and 2 noncanonical sites per dimer,[39] but it apparently displays a lower ligand affinity than Cpl1, with only 5 sites per dimer.[21,22] Our results obtained with the CBMs confirm these

https://dx.doi.org/10.1021/acsinfecdis.9b00344
ACS Infect. Dis. 2020, 6, 954−974

observations as the affinity of C-CbpD for choline (4 binding sites per monomer, Figures 3 and 5) is even higher than that of C-Cpl1 (5 binding sites per dimer, Figure 5). Nevertheless, it should be taken into account that the actual substrate of CBMs is the cell wall, which contains multiple copies of choline distributed along this supramolecular structure, leading to multivalency effects. So far, no affinity studies of CBPs have taken this into consideration, most likely due to the inherent inhomogeneities in different cell wall preparations. Therefore, we decided, for the first time, to use two defined, supramolecular cell-wall mimics (DEAE-MNPs and SPR DEAPA chips) to evaluate the binding strength of CBMs. Table 1 shows that the binding affinity to these substrates increases by a factor of 20−500 compared to free choline, with dissociation constants dropping from the millimolar to the micromolar range (Figures 7 and 8). The multivalent surface display is crucial for many biological interactions.[65] Its effect is widely recognized as an important strategy to improve affinity and specificity for biological targets.[66,67] In fact, we have previously proven that dendrimeric cell-wall mimics containing 4−64 choline molecules per particle display an affinity to CBMs several orders of magnitude higher than monovalent choline.[26] The comparative study among the tested CBMs shows that both C-Cpl1 and C-CbpD have a greater affinity to the macromolecular substrates than C-LytA, despite this polypeptide harboring more choline-binding sites (Table 1). This is in agreement with our previous observation that C-Cpl1 is also a more efficient inhibitor *in vitro* of the activity of parental LytA and Cpl1 hydrolases.[31] On the other hand, the engineered LZ-C-LytA oligomer, displaying the CBRs in a branched, rather than linear, fashion (Figure S3), also demonstrated an enhancement in affinity to SPR matrices compared to C-LytA alone (Figure 8 and Table 1). All these results strongly suggest that, despite the high sequence similarity displayed among most CBRs described so far, the biophysical basis of choline recognition in the cell wall by CBPs is a complex phenomenon which deserves further structural studies.

The affinity data discussed above, overall, can be translated to the effect of CBMs on pneumococcal planktonic cultures: both C-Cpl1 and C-CbpD caused an appreciable inhibition of CBP action (formation of long chains) and subsequent cell clumping at lower concentrations than the C-LytA protein (Figure 10), but the effect was most evident with LZ-C-LytA, which also displayed the strongest binding to SPR DEAPA chips (Figure 8 and Table 1), as well as the strongest stimulation of phagocytosis by macrophages (Figure 11). These results validate the use of DEAE-MNPs and DEAPA chips as suitable, defined *in vitro* models of the pneumococcal cell wall regarding choline disposition, which may be employed for the design and evaluation of novel variants.

Induction of cell aggregates suggests a second role of isolated CBMs as noncovalent agglutinating agents between the cells, leading to sedimentation. This is likely to be due to a thorough coating of the cell envelope by the protein added, increasing the hydrophobicity of the surface. In fact, a detailed inspection of the surface properties of the three tested CBMs (Figure 2B) reveals a certain degree of amphipathicity in their structures, with the presence of extensive hydrophobic patches that may lead to nonspecific protein−protein associations among adsorbed CBMs. Alternatively, due the solenoid shape of CBMs that allows the distribution of choline-binding sites all around the peptide chain (Figure 2A), there is also the possibility that a single CBM molecule binds to choline residues provided by two different cells, thus leading to flocculation. These possibilities are summarized in Figure S4. These cell clusters were more readily phagocytosed by mouse peritoneal macrophages than untreated pneumococci (Figure 11). This points to the CBMs as a possible novel family of antimicrobial agents for the management of pneumococcal infection by activating the natural host defense response (by inducing the phagocytosis of cell aggregates) as well as presumably blocking bacterial dissemination and favoring complement deposition (by promoting cell chains)[32] and preventing adhesion (for instance by displacing the CbpA adhesin), without any of the possible drawbacks derived from noncontrolled cellular lysis. In this sense, it has been demonstrated that agglutinating antibodies are more effective than nonagglutinating ones at promoting bacterial clearance in systemic infection models,[68] and much earlier observations reported that administration of pneumococci to immunized rabbits caused an almost immediate bacterial aggregation and clearance.[69] Therefore, CBMs could represent a type of antibody-like molecule specifically aimed to the pneumococcal surface that might also be used in biomedical applications such as diagnosis and directed drug delivery. Besides, full-length CBP enzymes have been successfully assayed in multiple occasions as efficient antipneumococcal molecules in animal models,[18] demonstrating that their choline-binding modules must be stable and nontoxic at least in the tested conditions. Taking into account that the CBMs employed in this work are natural modules (with the exception of LZ-C-LytA) not optimized for a strong binding to the cell wall, these polypeptides are susceptible to being further improved in their stabilities and binding affinities by protein engineering procedures, so as to became a therapeutically attractive antipneumococcal alternative.

CONCLUSIONS

The affinity of pneumococcal choline-binding modules (C-Cpl1, C-CbpD, C-LytA) for choline or pneumococcal cell-wall mimics is not directly related to the number of binding sites or their native oligomeric state. Theoretical studies and thermodynamic characterization of the protein−ligand interaction support the existence of noncanonical binding sites in both C-Cpl1 and C-CbpD. Moreover, the affinities of these modules for their macromolecular substrates may be substantially enhanced by rationally engineering their oligomerization (LZ-C-LytA protein) thanks to multivalence effects. These *in vitro* results have been extrapolated to a biological environment, as CBMs exogenously added to planktonic cultures recognize, in nanomolar concentrations, the choline residues in the pneumococcal cell wall, displacing the choline-binding proteins of the bacterial host and inducing chain formation and cell aggregates that foster their phagocytosis by macrophages. Both cell-clumping and phagocytosis-enhancing activities are closely related to the binding strength of CBMs to their macromolecular substrates *in vitro*. CBMs constitute, therefore, a suitable system to recognize and immobilize pneumococcal cells and represent a potential alternative to combat antimicrobial resistance issues by activating the natural defenses while avoiding any possible negative effects of bacterial lysis.

https://dx.doi.org/10.1021/acsinfecdis.9b00344
ACS Infect. Dis. 2020, 6, 954−974

METHODS

Reagents. Choline chloride and DEAE-cellulose were obtained from Sigma-Aldrich. Owing to the hygroscopic properties of choline, concentrated stock solutions were prepared from a freshly opened bottle and stored in aliquots at −20 °C. Isopropyl β-D-1-thiogalactopyranoside (IPTG) was purchased from Apollo Scientific (UK). Magnetic nanoparticles (MNPs) functionalized with *N*,*N*-diethylethanolamine (DEAE)-starch (200 nm) were purchased from Chemicell.

Bacterial Strains and Growth Conditions. The *Escherichia coli* strains were RB791[70] and BL21(DE3) (Novagen) and the cultures were grown with aeration in LB medium or in LB plus ampicillin (100 $\mu g/mL^{-1}$) when required.[71]

The *S. pneumoniae* strains used in this work were R6, a nonencapsulated strain derived from the capsular type 2 clinical isolate strain D39,[72] and R6CIB17, a R6 spontaneous mutant strain with a nonflocculant phenotype isolated in the laboratory of Profs. Ernesto García and Pedro García (CIB, CSIC, Spain), and whose whole-genome sequence was determined by Macrogen (Seoul, Korea) using a HiSeq sequencer and the TruSeq Nano DNA Kit (Illumina) (GenBank accession number: CP038808). Pneumococcal liquid cultures were grown at 37 °C without aeration in C medium supplemented with 0.08% (w/v) yeast extract (C+Y medium).[73] Growth was monitored by measuring the optical density at 550 nm (OD_{550}) in an Evolution 201 spectrophotometer (Thermo Scientific). Prior to every measurement, tubes were normally turned over several times to homogenize the solution, except when the flocculating capacity of additives was being assayed.

The number of viable cells was determined by counting the colonies appeared from appropriate dilutions of culture (in triplicate) after overnight incubation at 37 °C on trypticase soy plates (Conda-Pronadisa) supplemented with 5% defibrinated sheep blood (Thermo-Fisher).

Three-Dimensional Modeling of C-CbpD. A tertiary structure model of C-CbpD was generated by the SwissModel utilities (https://swissmodel.expasy.org/).[43] The best template encompassed the residues 234−331 of the pneumococcal CbpJ protein (PDB code 6JYX).[44]

In silico docking of choline molecules was accomplished as follows: a PDB file of choline was created with the ChemOffice 10.0 utilities (CambridgeSoft, U.K.) and, together with the template, prepared for docking using the UCSF Chimera 1.10 package (Resource for Biocomputing, Visualization, and Informatics at the University of California, San Francisco—supported by NIGMS P41-GM103311).[74] Both target and ligand files were submitted to the SwissDock server (http://www.swissdock.ch/).[45] Conformations showing occupancy of the four presumed binding sites and with the lowest calculated energy, were selected, and their coordinates added to those of the template into a single PDB file.

Expression and Purification of Proteins. C-LytA and C-Cpl1 proteins were overexpressed in *E. coli* RB791 from plasmids pCE17 and pCM1 plasmids as previously described.[31] Recombinant plasmids for the overproduction of C-CbpD (pET-*ccbp*D) and LZ-C-LytA (pET-lz*cclyt*A) were synthesized by GenScript (New Jersey, USA). For C-CbpD, a codon-optimized synthetic nucleotide sequence corresponding to amino acids from 353 to 448 of parental CbpD protein from the R6 strain was inserted between the *Nco*I and *Xho*I restriction sites of plasmid pET21d(+) (Novagen). Regarding LZ-C-LytA, a codon-optimized synthetic nucleotide sequence corresponding to the 106−142 region belonging to the PhaF phasin from *Pseudomonas putida* KT2440, which contains a leucine-zipper motif involved in oligomerization,[58,59] was fused upstream of the coding sequence for the C-LytA module as that expressed from pCE17 plasmid[31] and subsequently cloned into the pET21d(+) vector between the *Nco*I and *Xho*I restriction sites. In both constructions, three termination codons were introduced just before the *Xho*I site. For the overproduction of C-CbpD and LZ-C-LytA, *E. coli* BL21-(DE3) cells harboring either the pET-*ccbp*D or pET-lz*cclyt*A plasmid were cultured at 37 °C in LB medium to an OD_{600} of 0.6. Expression was then induced by the addition of 0.5 mM IPTG for 3 h at 30 °C, and then cells were harvested and disrupted using a Branson sonifier.

Purification of all CBMs from crude extracts was accomplished by affinity chromatography on DEAE-cellulose as described before.[31,52] The proteins were selectively eluted from the DEAE-cellulose column with 20 mM sodium phosphate buffer pH 7.0 plus 143 mM choline, dialyzed at 4 °C against 20 mM sodium phosphate buffer pH 7.0 to remove the ligand used for elution and stored at −20 °C. In the case of LZ-C-LytA, to prevent protein precipitation, dialysis of the protein was performed at a maximum concentration of 8 μM against phosphate buffer with gradually decreasing choline concentrations down to 10 mM, since the protein was highly insoluble in the absence of choline. For SPR experiments, a diluted sample of LZ-C-LytA (maximum 4 μM) was dialyzed against 10 mM ammonium hydrogen carbonate, centrifuged, and subsequently lyophilized.

Protein concentration was determined spectrophotometrically (Evolution 201, Thermo Scientific) using a molar extinction coefficient at 280 nm (ε_{280}) of 62540, 58900, 81076, and 67380 M^{-1} cm^{-1} for C-LytA, C-CbpD, C-Cpl1, and LZ-C-LytA, respectively.

Analytical Ultracentrifugation. Sedimentation velocity experiments were carried out by spinning the protein solution (0.85−5.5 μM) in a 20 mM sodium phosphate buffer, pH 7.0 in the absence or in the presence of 10 mM choline at 48,000 rpm and 20 °C in an XLI analytical ultracentrifuge (Beckman-Coulter Inc.) with UV−vis optical detection system, using an An50Ti rotor and 12 mm double-sector centerpieces. Sedimentation profiles were registered every 5 min at 230 nm in the case of C-Cpl1 and C-CbpD proteins and at 280 nm in the case of LZ-C-LytA. The sedimentation coefficient distributions were calculated by least-squares boundary modeling of sedimentation velocity data using the c(s) method, as implemented in the SEDFIT program.[75] These s-values were corrected to standard conditions (water, 20 °C, and infinite dilution)[76] using the SEDNTERP program to get the corresponding standard s-values ($s_{20,w}$).[77]

Circular Dichroism Spectroscopy (CD). CD-monitored thermal denaturation experiments were carried out in a Jasco J-815 spectropolarimeter (Tokyo, Japan) equipped with a Peltier PTC-423S and using a cuvette path-length of 0.1 cm. All measurements were carried out in quadruplicate at 20 °C in the presence 20 mM sodium phosphate buffer at pH 7.0. Protein concentration was 0.1 mg mL^{-1}. The sample was layered with mineral oil to avoid evaporation, and the heating rate was 60 °C h^{-1}. After subtracting the baseline from the sample spectra, CD data were processed with the adaptive

https://dx.doi.org/10.1021/acsinfecdis.9b00344
ACS Infect. Dis. 2020, 6, 954−974

smoothing method provided by the Jasco Spectra Analysis software. Molar ellipticities ($[\theta]$) were expressed in deg cm^2 (dmol of residues)$^{-1}$.

The thermal scans were fitted by least-squares to the Gibbs–Helmholtz eq (eq 1):

$$\Delta G^o(T) = \Delta H_m(1 - {}^{T}/_{T_m}) - \Delta C_p[(T_m - T) + T \ln({}^{T}/_{T_m})] \quad (1)$$

where ΔG^o (T) is the free energy of the protein at a temperature T, ΔH_m is the van't Hoff enthalpy, T_m is the midpoint of denaturation (in Kelvin), and ΔC_p is the difference in heat capacity between the native and denatured states.

For ΔC_p estimation, several procedures were followed. The rule-of-thumb approach by Pace (1989)[49] is the simplest one and assigns an average value per residue (eq 2):

$$\Delta C_p = 12n \quad (2)$$

where the units of ΔC_p are kcal mol^{-1} K^{-1} and n is the number of residues.

The methods by Spolar et al. (eq 3)[51] and Myers et al. (eq 4)[50] make use of differences both in nonpolar (ΔASA_{np}) and polar (ΔASA_p) accessible surface area between the folded and the unfolded states:

$$\Delta C_p = 0.32(\Delta ASA_{np}) - 0.14(\Delta ASA_p) \quad (3)$$

$$\Delta C_p = 0.28(\Delta ASA_{np}) - 0.09(\Delta ASA_p) \quad (4)$$

where ΔASA is given in nm^2 and the units of ΔC_p are kcal mol^{-1} K^{-1}. In turn, to estimate ΔASA values, in a first step, three-dimensional theoretical structures of extended unfolded states were generated with SwissPDB viewer 4.1.0[78] by assigning β-structure Ramachandran angles to all residues. Then, the structures of both the folded and the unfolded conformations were submitted to the GetArea server (http://curie.utmb.edu/getarea.html).[79]

To ascertain the number of choline-binding sites for C-Cpl1 and C-CbpD proteins, thermal scans were performed at different saturating choline concentrations (see Figure 5). The number of sites was obtained from van't Hoff plots, making use of the van't Hoff equation:[47]

$$\ln([C]) = -({}^{\Delta H_m}/_{nR}) * {}^{1}/_{T_m} + {}^{\Delta S_m}/_{nR} \quad (5)$$

where $[C]$ is the molar choline concentration, T_m is the midpoint of denaturation (in Kelvin), ΔH_m and ΔS_m are the average van't Hoff enthalpy (as calculated with eq 1 for each point) and entropy changes at the midpoint, respectively, R is the gas constant, and n is the number of sites.

Fluorescence Spectroscopy. Fluorescence measurements were performed on a PTI-fluorimeter TI-Quanta Maser QM-62003SE (Birmingham, NJ, EE.UU) using a 5 × 5 mm path-length cuvette and a protein concentration of 1 μM in 20 mM sodium phosphate buffer at pH 7.0 and 20 °C. For choline titrations, aliquots from a 150 mM choline stock solution were added stepwise and incubated approximately for 5 min prior to measurement. Tryptophan emission spectra were obtained using an excitation wavelength of 280 nm and the emission was registered between 300 and 400 nm, using excitation and emission slits of 0.5 nm and a scan rate of 60 nm·min^{-1}.

The average emission intensity ($\langle\lambda\rangle$) of fluorescence spectra was calculated as depicted in eq 6:

$$\langle\lambda\rangle = {\sum_1^n (I_i\lambda_i)}\Big/{\sum_1^n I_i} \quad (6)$$

where I_i is the fluorescence intensity measured at wavelength λ_i.

The choline titration data for C-Cpl1 were fitted to eq 7, which is a modified version of that developed by Monterroso et al.,[21] but this time considering both dimer formation on choline binding and the presence of 5 choline-binding sites per dimer (see text for details):

$$|\Delta\langle\lambda\rangle| = ([M]^2 r(A + B) - p[D]_0)/[C] \quad (7)$$

in which the value of $[M]$, A, and B is described as follows:

$$[M] = \frac{(-1 + (1 + 8[C]r(1 + K_b[L])^5)^{1/2})}{(4r(1 + K_b[L])^5)}$$

$$A = p(1 + K_b[L])^5$$

$$B = 5h(K_b[L] + 4K_b{}^2[L]^2 + 6K_b{}^3[L]^3 + 4K_b{}^4[L]^4 + K_b{}^5[L]^5)$$

where $[M]$ is the concentration of the monomeric conformation of the protein; $[D]_0$ is the initial concentration of dimers in the absence of choline (assumed in our case to be negligible—see Figure 4); $[C]$ is the total protein concentration (in monomer moles); r is the dimerization constant in the absence of choline; p is the change in $|\langle\lambda\rangle|$ due to the dimerization of the protein in the absence of choline; K_b is the choline binding constant; and h is the change in $|\langle\lambda\rangle|$ due to binding of choline to the protein dimer (per mol of sites in each monomer). The choline dissociation constant (K_d) was then calculated as $1/K_b$.

The choline titration data for C-CbpD were fitted to a simple ligand binding model (eq 8), considering 4 independent binding sites of the same type:

$$|\Delta\langle\lambda\rangle| = \frac{4|\langle\lambda\rangle|_{max}[L]}{K_d + [L]} \quad (8)$$

where $|\langle\lambda\rangle|$ is the absolute change in average emission intensity at each ligand concentration, $|\langle\lambda\rangle|_{max}$ is the maximum change in average emission intensity per site on ligand saturation, and K_d is the dissociation constant.

Binding of CBMs to DEAE-Coated Magnetic Nanoparticles. FluidMAG magnetic nanoparticles functionalized with 2-diethylaminoethyl-starch groups (DEAE-MNPs) (200 nm diameter, Chemicell, Germany) were washed, equilibrated in 20 mM sodium phosphate, pH 7.0 and finally distributed in aliquots. Such aliquots were then incubated separately with 300 μL of 20 mM sodium phosphate, pH 7.0 containing increasing concentrations of C-LytA, C-CbpD, or C-Cpl1, to a final nanoparticle concentration of 0.25 mg mL^{-1} (approximately 5.5 × 10^{10} particles mL^{-1}). The incubation was maintained for 30 min at room temperature in a rotary mixer (Ovan). At this point, bound protein was separated from the solution using a magnet (MagnetoPURE) for 5 min. The supernatant was subsequently centrifuged for 3 min at 5000g in a miniSpin centrifuge (Eppendorf) to ensure the removal of residual MNPs, and the amount of unbound protein was measured spectrophotometrically. The amount of bound protein at each point was estimated by subtraction of the quantified unbound protein from the initial protein added in

https://dx.doi.org/10.1021/acsinfecdis.9b00344
ACS Infect. Dis. 2020, 6, 954–974

the assay. The protein binding on the surface of DEAE-MNP was analyzed by Langmuir analysis[80] (eq 9):

$$q = \frac{q_{max} \cdot [C]}{K_d + [C]} \quad (9)$$

where q is the amount of protein bound to the MNP at each protein concentration, q_{max} is the maximum adsorption capacity, $[C]$ is the initial protein concentration and K_d is the dissociation constant. Nonfunctionalized MNPs were assayed as controls for nonspecific binding, which was found to be negligible (data not shown). More details on the biophysical characterization of the specific binding of the CBMs to DEAE-MNPs will be published elsewhere.

Surface Plasmon Resonance Experiments (SPR). SPR experiments were performed at 25 °C with Biacore X-100 (GE) equipment. Carboxymethyldextran chips (CM5) (Biacore, GE) were used as support for immobilization of 3-diethylaminopropylamine. First, carboxymethylated groups were activated by injection of a 1:1 mixture of 0.4 M 1-ethyl-3-(3-(dimethylamino)propyl)-carbodiimide and 0.1 M *N*-hydroxysuccinimide at a flow rate of 10 μL min^{-1} for 7 min. Then, 3-diethylaminopropylamine was injected at 10 μL min^{-1}, using concentrations of 1−100 μM for 100 s to obtaining a response density of 250 response units. Finally, blockage of the remaining reactive groups was carried out by injection of 1 M ethanolamine pH 8.5 for 7 min (flow cell without ligand was used as reference).

Binding of CBMs in 20 mM sodium phosphate, pH 7.0 plus 0.005% Tween was measured by injection of increasing concentrations of each protein over the functionalized chip. The flow rate (V_f) and the association and dissociation periods (t_{as} and t_{dis}) for the different proteins tested are indicated in Table S3.

The binding affinity was determined by fitting the sensorgram curve obtained to a single hyperbole for LZ-C-LytA and C-Cpl1 (model with one type of CBSs, eq 10) and to a double hyperbole for C-LytA (model with two types of CBSs, eq 11).

$$R_{eq} = \frac{R_{max}[P]}{K_d + [P]} \quad (10)$$

$$R_{eq} = \frac{R_{max1}[P]}{K_{d1} + [P]} + \frac{R_{max2}[P]}{K_{d2} + [P]} \quad (11)$$

where R_{eq} is the response in the equilibrium (maximum experimental measurement for each point at different concentrations); $[P]$ is the protein concentration; R_{max} is the maximum surface-binding response for a single site type (calculated from the fitting); R_{max1} and R_{max2} are the maximum surface-binding response when considering two site types; K_d is the macroscopic dissociation constant for a single site type; and K_{d1} and K_{d2} are the dissociation constants when considering two site types.

Laser Scanning Confocal Microscopy (LSCM). At different times of growth, a sample of the pneumococcal liquid culture was taken and cells were stained with the LIVE/DEAD *Bac*Light bacterial viability kit (Molecular Probes) to monitor bacterial populations. A 3 μL mixture of 1:1 SYTO 9:propidium iodide mix was added to a 1 mL sample of the culture medium and kept at room temperature during 15 min in the dark. Confocal images were captured using an inverse laser scanning confocal microscope (Leika TCS-SP2-AOBS-UV) with a 63× oil-immersion lens. The excitation/emission wavelengths for SYTO 9 and propidium iodide were 488/500−550 nm and 543/600−670 nm, respectively.

Tertiary Structure Predictions for LZ-C-LytA Protein. Three-dimensional coordinates corresponding to the sequence containing the predicted leucine zipper of *Pseudomonas putida* PhaF phasin (LZ sequence: MGLGVPSRNEIKALHQQVDSLTKQIEKLTGASVTPISSRK) were taken from a previous PhaF model,[58] and those related to the C-LytA were obtained from the solved X-ray crystal structure (PDB code: 1HCX).[33] The SwissPDB Viewer 4.1 program[78] was used to connect both sequences and to generate the basic model of the LZ-C-LytA monomer and of the dimer linked through the C-LytA moiety (CT2 variant, see Table S2). Next, the monomeric LZ-C-LytA PDB file was submitted to the M-ZDOCK server (http://zdock.umassmed.edu/m-zdock/)[60] to generate the rest of the oligomer conformations involving interactions through the leucine zippers (LZ2-4 variants, Table S2). In those cases in which the server was not able to render the corresponding model, the isolated LZ sequence was submitted to the M-ZDOCK and the corresponding generated models were used in turn as templates for the alignment of the full-length monomer, making use of the "Iterative Fit" utility of SwissPDB Viewer 4.1. The LZ templates were subsequently removed from the final model.

The theoretical hydrodynamic properties for each model were estimated by using the HyproPro 10 program,[61] and using as parameters a disolvent density of 1 g mL^{-1}, viscosity of 0.01 P, temperature of 20 °C, and a specific volume 0.722 mL g^{-1} (taken from that described for C-LytA protein).[23]

Phagocytosis Assays. The animal experiments were approved by the Animal Care Committee of the University Hospital of Göttingen, Germany, and by the Niedersächsisches Landesamt für Verbraucherschutz and Lebensmittelsicherheit (LAVES), Braunschweig, Lower Saxony, Germany. The C57/BI6N mice (7 animals for C-Cpl1 and 5 for LzClytA experiments, all 10−14 weeks old) were sacrificed by CO_2 inhalation. Peritoneal lavage was performed twice with 5 mL of sterile and cool 10 mM phosphate buffered saline (PBS) (138 mM NaCl, 2.7 mM KCl, pH 7.4) using a 21-gauge needle. The peritoneal fluid was then collected and centrifuged for 8 min at 500*g* and 4 °C, and the pellet was washed twice with PBS. The final sediment was suspended in Dulbecco's modified Eagle's medium (DMEM) (Gibco, Karlsruhe, Germany) supplemented with 10% of heat-inactivated fetal calf serum (FCS), 100 U/mL^{-1} penicillin and 100 μg/mL^{-1} streptomycin. Cells were counted with a hemocytometer, plated in a 96-well plate at a density of 15 × 10^4 cells/well and maintained at 37 °C in a humidified atmosphere with 5% CO_2. After 48 h, the culture medium was changed to nonantibiotic conditions.

The pneumococcal culture (R6 strain) was grown in tryptic soy broth (Sigma-Aldrich) at 37 °C without agitation and in the presence of 5% CO_2. Bacterial growth was monitored by quantitative plating of viable bacteria (serial 10-fold dilutions performed in sterile saline solution were plated on blood agar, and the bacterial colonies in the appropriate dilutions were counted). The protein C-Cpl1 (18 μg/mL^{-1} in 20 mM sodium phosphate, pH 7.0) or LZ-C-LytA (20 μg/mL^{-1} in 20 mM sodium phosphate, pH 7.0) was added to the culture both from the beginning of the bacterial growth (coincubation time, 16 h) or at the late exponential phase (coincubation time, 2 h). A control was realized in each case by coincubation of the culture with 20 mM sodium phosphate, pH 7.0.

https://dx.doi.org/10.1021/acsinfecdis.9b00344
ACS Infect. Dis. 2020, 6, 954−974

A 200 μL sample of the pneumococcal culture previously treated with the respective protein was centrifuged at room temperature for 5 min at 1000*g*, and the pellet was suspended in the same volume of DMEM medium suplemented with 10% FCS. The bacteria were added to the macrophages in a ratio of approximately 100 bacteria per phagocyte (1.5×10^7 CFU/well) and coincubated for 1 h at 37 °C in a humidified atmosphere with 5% CO_2. Next, the macrophages were washed twice with 0.9% NaCl, resuspended in DMEM medium supplemented with 10% FCS and 100 mg/mL^{-1} gentamicin (Sigma-Aldrich) and incubated for 1 h at 37 °C in the presence of 5% CO_2 in order to kill the ramaining extracellular bacteria. Finally, the macrophages were washed twice with 0.9% NaCl and lysed by addition of 100 μL of distilled water. The bacteria were then quantified by quantitative plating of viable bacteria as described above.

The statistical analysis was carried out using GraphPad Prism (GraphPad 6 Software, San Diego, CA, USA). Data were expressed as medians (25th percentile/75th percentile). Kruskal–Wallis test followed by Dunn's multiple comparison test was used to compare data. Probabilities lower than 0.05 were considered statistically significant (****, $p < 0.0001$).

■ ASSOCIATED CONTENT

Supporting Information

The Supporting Information is available free of charge at https://pubs.acs.org/doi/10.1021/acsinfecdis.9b00344.

Figure S1. Intrinsic fluorescence emission spectra of C-Cpl1 (A) and C-CbpD (B) in phosphate buffer (black) plus 20 mM NaCl (green) or 20 mM choline chloride (red); Spectra registered at various choline concentrations for C-Cpl1 (C) and C-CbpD (D). Figure S2. Planktonic culture in the stationary phase of *S. pneumoniae* R6CIB17 in the absence (left) and the presence (right) of C-LytA 1 μM. Figure S3. (Upper panel) amino acid sequence and structural model of the monomer of the LZ-C-LytA protein. Sequence derived from the PhaF phasin is shown in blue, with the predicted leucine-zipper motif underlined. (Lower panels) three-dimensional models of LZ-C-LytA oligomers. CT species, dimerization through the C-terminal hairpin of C-LytA; LZ species, oligomerization through the leucine zipper sequence. Figure S4. Possible models for CBM-induced *S. pneumoniae* agglutination. Table S1. Theoretical estimation of ΔC_p values for C-Cpl1 and C-CbpD proteins. ΔASA values were calculated from PDB files with the GetArea utilities.[79] Table S2. Theoretical prediction of the hydrodynamic properties of modeled LZ-C-LytA oligomers. Table S3. Conditions of SPR experiments. V_f, flow rate; t_{as}, association time; t_{dis}, dissociation time. (PDF)

■ AUTHOR INFORMATION

Corresponding Authors

Jesús M. Sanz − *Institute of Research, Development, and Innovation in Healthcare Biotechnology in Elche (IDiBE), Miguel Hernández University, Elche 03202, Spain; Biological Research Centre, Spanish National Research Council (CSIC), Madrid 28040, Spain; Centro de Investigación Biomédica en Red de Enfermedades Respiratorias (CIBERES), Madrid 28040, Spain*; Email: jmsanz@cib.csic.es

Beatriz Maestro − *Institute of Research, Development, and Innovation in Healthcare Biotechnology in Elche (IDiBE), Miguel Hernández University, Elche 03202, Spain; Biological Research Centre, Spanish National Research Council (CSIC), Madrid 28040, Spain*; orcid.org/0000-0001-5317-650X; Email: bmaestro35@gmail.com

Authors

Emma Roig-Molina − *Institute of Research, Development, and Innovation in Healthcare Biotechnology in Elche (IDiBE), Miguel Hernández University, Elche 03202, Spain*

Manuel Sánchez-Angulo − *Department of Vegetal Production and Microbiology, Miguel Hernández University, Elche 03202, Spain*

Jana Seele − *Department of Geriatrics, Evangelisches Krankenhaus Göttingen-Weende, 37075 Göttingen, Germany; Department of Neuropathology, University Medical Center Göttingen, 37073 Göttingen, Germany*

Francisco García-Asencio − *Institute of Research, Development, and Innovation in Healthcare Biotechnology in Elche (IDiBE), Miguel Hernández University, Elche 03202, Spain*

Roland Nau − *Department of Geriatrics, Evangelisches Krankenhaus Göttingen-Weende, 37075 Göttingen, Germany; Department of Neuropathology, University Medical Center Göttingen, 37073 Göttingen, Germany*

Complete contact information is available at: https://pubs.acs.org/10.1021/acsinfecdis.9b00344

Author Contributions

$^{\nabla}$J.M.S. and B.M. contributed equally to this work. Conceived and designed the experiments: ER-M, MS-A, JS, RN, JMS, BM. Performed the experiments: ER-M, MS-A, JS, FG-A, BM. Analyzed the data: RN, JMS, BM. Contributed reagents/materials/analysis tools: RN, JMS. Wrote the paper: JS, RN, JMS, BM. Contributed with ideas: ER-M, MS-A.

Notes

The authors declare no competing financial interest.

■ ACKNOWLEDGMENTS

We thank Cristina Almansa (confocal microscopy), Laura Lagartera (SPR experiments), Juan R. Luque (analytical ultracentrifugation), and M. Garzón for skillful technical assistance. We especially thank M. Menéndez and P. García for helpful discussions. This work was supported by grants from the Spanish Ministry of Economy, Industry and Competitiveness (BIO2013-47684-R and BIO2016-79323-R), the RETICS-FEDER RICET RD16/0027/0010 (Spain), and the B. Braun Foundation, Melsungen, Germany. The CIBER de Enfermedades Respiratorias (CIBERES) is an initiative of the Spanish Instituto de Salud Carlos III. We acknowledge support of the publication fee by the CSIC Open Access Publication Support Initiative through its Unit of Information Resources for Research (URICI).

■ REFERENCES

(1) O'Brien, K. L., Wolfson, L. J., Watt, J. P., Henkle, E., Deloria-Knoll, M., McCall, N., Lee, E., Mulholland, K., Levine, O. S., and Cherian, T. (2009) Hib and Pneumococcal Global Burden of Disease Study Team, Burden of disease caused by *Streptococcus pneumoniae* in children younger than 5 years: global estimates. *Lancet* 374 (9693), 893–902.

(2) Rodrigues, C. M. C., and Groves, H. (2018) Community-Acquired Pneumonia in Children: the Challenges of Microbiological Diagnosis. *J. Clin. Microbiol. 56* (3), DOI: 10.1128/JCM.01318-17.
(3) UNICEF. (2006) *Pneumonia: The Forgotten Killer of Children*, United Nations Children's Emergency Fund, New York, NY, USA.
(4) (2018) Global Burden of Disease Lower Respiratory Infections Collaborators, Estimates of the global, regional, and national morbidity, mortality, and aetiologies of lower respiratory infections in 195 countries, 1990−2016: a systematic analysis for the Global Burden of Disease Study 2016. *Lancet Infect. Dis. 18* (11), 1191−1210. .
(5) Tacconelli, E., Carrara, E., Savoldi, A., Harbarth, S., Mendelson, M., Monnet, D. L., Pulcini, C., Kahlmeter, G., Kluytmans, J., Carmeli, Y., Ouellette, M., Outterson, K., Patel, J., Cavaleri, M., Cox, E. M., Houchens, C. R., Grayson, M. L., Hansen, P., Singh, N., Theuretzbacher, U., and Magrini, N. (2018) W. H. O. Pathogens Priority List Working Group, Discovery, research, and development of new antibiotics: the WHO priority list of antibiotic-resistant bacteria and tuberculosis. *Lancet Infect. Dis. 18* (3), 318−327.
(6) Centers for Disease Control and Prevention. (2013) *Antibiotic resistance threats in the United States*, U.S. Department of Health.
(7) Geno, K. A., Gilbert, G. L., Song, J. Y., Skovsted, I. C., Klugman, K. P., Jones, C., Konradsen, H. B., and Nahm, M. H. (2015) Pneumococcal Capsules and Their Types: Past, Present, and Future. *Clin. Microbiol. Rev. 28* (3), 871−99.
(8) Papadatou, I., and Spoulou, V. (2016) Pneumococcal Vaccination in High-Risk Individuals: Are We Doing It Right? *Clin. Vaccine Immunol. 23* (5), 388−395.
(9) Alexandre, C., Dubos, F., Courouble, C., Pruvost, I., and Varon, E. (2010) Hospital Network for Evaluating the Management of Common Childhood, D.; Martinot, A., Rebound in the incidence of pneumococcal meningitis in northern France: effect of serotype replacement. *Acta Paediatr 99* (11), 1686−90.
(10) Weil-Olivier, C., van der Linden, M., de Schutter, I., Dagan, R., and Mantovani, L. (2012) Prevention of pneumococcal diseases in the post-seven valent vaccine era: a European perspective. *BMC Infect. Dis. 12*, 207.
(11) Koelman, D. L. H., Brouwer, M. C., and van de Beek, D. (2020) Resurgence of pneumococcal meningitis in Europe and Northern America. *Clin. Microbiol. Infect. 26*, 199.
(12) WHO/UNICEF. (2016) *The WHO/UNICEF estimates of national immunization coverage (WUENIC)*.
(13) Johns Hopkins Bloomberg School of Public Health International Vaccine Access Center (IVAC). (2018) *VIEW-hub Report: Global Vaccine Introduction and Implementation*.
(14) Todorova, K., Maurer, P., Rieger, M., Becker, T., Bui, N. K., Gray, J., Vollmer, W., and Hakenbeck, R. (2015) Transfer of penicillin resistance from *Streptococcus oralis* to *Streptococcus pneumoniae* identifies *murE* as resistance determinant. *Mol. Microbiol. 97* (5), 866−80.
(15) Cherazard, R., Epstein, M., Doan, T. L., Salim, T., Bharti, S., and Smith, M. A. (2017) *Antimicrobial Resistant Streptococcus pneumoniae*: Prevalence, Mechanisms, and Clinical Implications. *Am. J. Ther. 24* (3), e361−e369.
(16) European Centre for Disease Prevention and Control (ECDC). (2017) *Surveillance of antimicrobial resistance in Europe*.
(17) Pérez-Dorado, I., Galán-Bartual, S., and Hermoso, J. A. (2012) Pneumococcal surface proteins: when the whole is greater than the sum of its parts. *Mol. Oral Microbiol. 27* (4), 221−45.
(18) Maestro, B., and Sanz, J. M. (2016) Choline Binding Proteins from *Streptococcus pneumoniae*: A Dual Role as Enzybiotics and Targets for the Design of New Antimicrobials. *Antibiotics (Basel, Switz.) 5* (2), 21.
(19) Giudicelli, S., and Tomasz, A. (1984) Attachment of pneumococcal autolysin to wall teichoic acids, an essential step in enzymatic wall degradation. *J. Bacteriol. 158* (3), 1188−90.
(20) Briese, T., and Hakenbeck, R. (1985) Interaction of the pneumococcal amidase with lipoteichoic acid and choline. *Eur. J. Biochem. 146* (2), 417−27.
(21) Monterroso, B., Saiz, J. L., Garcia, P., Garcia, J. L., and Menendez, M. (2008) Insights into the structure-function relationships of pneumococcal cell wall lysozymes, LytC and Cpl-1. *J. Biol. Chem. 283* (42), 28618−28.
(22) Medrano, F. J., Gasset, M., Lopez-Zumel, C., Usobiaga, P., Garcia, J. L., and Menéndez, M. (1996) Structural characterization of the unligated and choline-bound forms of the major pneumococcal autolysin LytA amidase. Conformational transitions induced by temperature. *J. Biol. Chem. 271* (46), 29152−61.
(23) Usobiaga, P., Medrano, F. J., Gasset, M., García, J. L., Saiz, J. L., Rivas, G., Laynez, J., and Menéndez, M. (1996) Structural organization of the major autolysin from Streptococcus pneumoniae. *J. Biol. Chem. 271* (12), 6832−8.
(24) Sanz, J. M., García, J. L., Laynez, J., Usobiaga, P., and Menéndez, M. (1993) Thermal stability and cooperative domains of CPL1 lysozyme and its NH2- and COOH-terminal modules. Dependence on choline binding. *J. Biol. Chem. 268* (9), 6125−30.
(25) Maestro, B., González, A., García, P., and Sanz, J. M. (2007) Inhibition of pneumococcal choline-binding proteins and cell growth by esters of bicyclic amines. *FEBS J. 274* (2), 364−76.
(26) Hernández-Rocamora, V. M., Maestro, B., de Waal, B., Morales, M., García, P., Meijer, E. W., Merkx, M., and Sanz, J. M. (2009) Multivalent choline dendrimers as potent inhibitors of pneumococcal cell-wall hydrolysis. *Angew. Chem., Int. Ed. 48* (5), 948−51.
(27) Ribes, S., Riegelmann, J., Redlich, S., Maestro, B., de Waal, B., Meijer, E. W., Sanz, J. M., and Nau, R. (2013) Multivalent choline dendrimers increase phagocytosis of *Streptococcus pneumoniae* R6 by microglial cells. *Chemotherapy 59* (2), 138−42.
(28) Nau, R., and Eiffert, H. (2005) Minimizing the release of proinflammatory and toxic bacterial products within the host: a promising approach to improve outcome in life-threatening infections. *FEMS Immunol. Med. Microbiol. 44* (1), 1−16.
(29) Brown, L. A., Mitchell, A. M., and Mitchell, T. J. (2017) *Streptococcus pneumoniae* and lytic antibiotic therapy: are we adding insult to injury during invasive pneumococcal disease and sepsis? *J. Med. Microbiol. 66*, 1253.
(30) Martner, A., Skovbjerg, S., Paton, J. C., and Wold, A. E. (2009) *Streptococcus pneumoniae* autolysis prevents phagocytosis and production of phagocyte-activating cytokines. *Infect. Immun. 77* (9), 3826−37.
(31) Sánchez-Puelles, J. M., Sanz, J. M., García, J. L., and García, E. (1990) Cloning and expression of gene fragments encoding the choline-binding domain of pneumococcal murein hydrolases. *Gene 89* (1), 69−75.
(32) Dalia, A. B., and Weiser, J. N. (2011) Minimization of bacterial size allows for complement evasion and is overcome by the agglutinating effect of antibody. *Cell Host Microbe 10* (5), 486−96.
(33) Fernández-Tornero, C., López, R., García, E., Giménez-Gallego, G., and Romero, A. (2001) A novel solenoid fold in the cell wall anchoring domain of the pneumococcal virulence factor LytA. *Nat. Struct. Biol. 8* (12), 1020−4.
(34) Maestro, B., and Sanz, J. M. (2005) Accumulation of partly folded states in the equilibrium unfolding of the pneumococcal choline-binding module C-LytA. *Biochem. J. 387* (Pt 2), 479−88.
(35) Guiral, S., Mitchell, T. J., Martin, B., and Claverys, J. P. (2005) Competence-programmed predation of noncompetent cells in the human pathogen Streptococcus pneumoniae: genetic requirements. *Proc. Natl. Acad. Sci. U. S. A. 102* (24), 8710−5.
(36) García, J. L., García, E., Arrarás, A., García, P., Ronda, C., and López, R. (1987) Cloning, purification, and biochemical characterization of the pneumococcal bacteriophage Cp-1 lysin. *J. Virol. 61* (8), 2573−80.
(37) Hermoso, J. A., Monterroso, B., Albert, A., Galán, B., Ahrazem, O., García, P., Martínez-Ripoll, M., García, J. L., and Menéndez, M. (2003) Structural basis for selective recognition of pneumococcal cell wall by modular endolysin from phage Cp-1. *Structure 11* (10), 1239−49.
(38) Pérez-Dorado, I., González, A., Morales, M., Sanles, R., Striker, W., Vollmer, W., Mobashery, S., García, J. L., Martínez-Ripoll, M.,

García, P., and Hermoso, J. A. (2010) Insights into pneumococcal fratricide from the crystal structures of the modular killing factor LytC. *Nat. Struct. Mol. Biol. 17* (5), 576−81.
(39) Li, Q., Cheng, W., Morlot, C., Bai, X. H., Jiang, Y. L., Wang, W., Roper, D. I., Vernet, T., Dong, Y. H., Chen, Y., and Zhou, C. Z. (2015) Full-length structure of the major autolysin LytA. *Acta Crystallogr., Sect. D: Biol. Crystallogr. 71* (Pt 6), 1373−81.
(40) García, E., García, J. L., García, P., Arrarás, A., Sánchez-Puelles, J. M., and López, R. (1988) Molecular evolution of lytic enzymes of *Streptococcus pneumoniae* and its bacteriophages. *Proc. Natl. Acad. Sci. U. S. A. 85* (3), 914−8.
(41) Buey, R. M., Monterroso, B., Menéndez, M., Diakun, G., Chacón, P., Hermoso, J. A., and Díaz, J. F. (2007) Insights into molecular plasticity of choline binding proteins (pneumococcal surface proteins) by SAXS. *J. Mol. Biol. 365* (2), 411−24.
(42) Gosink, K. K., Mann, E. R., Guglielmo, C., Tuomanen, E. I., and Masure, H. R. (2000) Role of novel choline binding proteins in virulence of *Streptococcus pneumoniae*. *Infect. Immun. 68* (10), 5690−5.
(43) Waterhouse, A., Bertoni, M., Bienert, S., Studer, G., Tauriello, G., Gumienny, R., Heer, F. T., de Beer, T. A. P., Rempfer, C., Bordoli, L., Lepore, R., and Schwede, T. (2018) SWISS-MODEL: homology modelling of protein structures and complexes. *Nucleic Acids Res. 46* (W1), W296−W303.
(44) Xu, Q., Zhang, J. W., Chen, Y., Li, Q., and Jiang, Y. L. (2019) Crystal structure of the choline-binding protein CbpJ from Streptococcus pneumoniae. *Biochem. Biophys. Res. Commun. 514* (4), 1192−1197.
(45) Grosdidier, A., Zoete, V., and Michielin, O. (2011) SwissDock, a protein-small molecule docking web service based on EADock DSS. *Nucleic Acids Res. 39* (Web Server issue), W270−7.
(46) Greenfield, N. J. (2006) Using circular dichroism collected as a function of temperature to determine the thermodynamics of protein unfolding and binding interactions. *Nat. Protoc. 1* (6), 2527−35.
(47) Fukada, H., Sturtevant, J. M., and Quiocho, F. A. (1983) Thermodynamics of the binding of L-arabinose and of D-galactose to the L-arabinose-binding protein of Escherichia coli. *J. Biol. Chem. 258* (21), 13193−8.
(48) Freire, E., van Osdol, W. W., Mayorga, O. L., and Sánchez-Ruiz, J. M. (1990) Calorimetrically determined dynamics of complex unfolding transitions in proteins. *Annu. Rev. Biophys. Biophys. Chem. 19*, 159−88.
(49) Pace, C. N., and Scholtz, J. M. Measuring the conformational stability of a protein. (1989) in *Protein Structure: A Practical Approach* (Creighton, T. E., Ed.), pp 299−321, Oxford University Press.
(50) Myers, J. K., Pace, C. N., and Scholtz, J. M. (1995) Denaturant m values and heat capacity changes: relation to changes in accessible surface areas of protein unfolding. *Protein Sci. 4* (10), 2138−48.
(51) Spolar, R. S., Livingstone, J. R., and Record, M. T., Jr. (1992) Use of liquid hydrocarbon and amide transfer data to estimate contributions to thermodynamic functions of protein folding from the removal of nonpolar and polar surface from water. *Biochemistry 31* (16), 3947−55.
(52) Sanz, J. M., López, R., and García, J. L. (1988) Structural requirements of choline derivatives for 'conversion' of pneumococcal amidase. A new single-step procedure for purification of this autolysin. *FEBS Lett. 232* (2), 308−12.
(53) Sánchez-Puelles, J. M., Sanz, J. M., García, J. L., and García, E. (1992) Immobilization and single-step purification of fusion proteins using DEAE-cellulose. *Eur. J. Biochem. 203* (1−2), 153−9.
(54) Silva-Martin, N., Retamosa, M. G., Maestro, B., Bartual, S. G., Rodes, M. J., García, P., Sanz, J. M., and Hermoso, J. A. (2014) Crystal structures of CbpF complexed with atropine and ipratropium reveal clues for the design of novel antimicrobials against *Streptococcus pneumoniae*. *Biochim. Biophys. Acta, Gen. Subj. 1840* (1), 129−35.
(55) Maestro, B., Velasco, I., Castillejo, I., Arévalo-Rodriguez, M., Cebolla, A., and Sanz, J. M. (2008) Affinity partitioning of proteins tagged with choline-binding modules in aqueous two-phase systems. *J. Chromatogr. A 1208* (1−2), 189−96.
(56) De Las Rivas, B., García, J. L., López, R., and García, P. (2002) Purification and polar localization of pneumococcal LytB, a putative endo-beta-N-acetylglucosaminidase: the chain-dispersing murein hydrolase. *J. Bacteriol. 184* (18), 4988−5000.
(57) Retamosa, M. G., Díez-Martínez, R., Maestro, B., García-Fernández, E., de Waal, B., Meijer, E. W., García, P., and Sanz, J. M. (2015) Aromatic Esters of Bicyclic Amines as Antimicrobials against *Streptococcus pneumoniae*. *Angew. Chem., Int. Ed. 54* (46), 13673−7.
(58) Maestro, B., Galán, B., Alfonso, C., Rivas, G., Prieto, M. A., and Sanz, J. M. (2013) A new family of intrinsically disordered proteins: structural characterization of the major phasin PhaF from *Pseudomonas putida* KT2440. *PLoS One 8* (2), e56904.
(59) Tarazona, N. A., Maestro, B., Revelles, O., Sanz, J. M., and Prieto, M. A. (2019) Role of leucine zipper-like motifs in the oligomerization of *Pseudomonas putida* phasins. *Biochim. Biophys. Acta, Gen. Subj. 1863* (2), 362−370.
(60) Pierce, B. G., Wiehe, K., Hwang, H., Kim, B. H., Vreven, T., and Weng, Z. (2014) ZDOCK server: interactive docking prediction of protein-protein complexes and symmetric multimers. *Bioinformatics 30* (12), 1771−3.
(61) Ortega, A., Amorós, D., and García de la Torre, J. (2011) Prediction of hydrodynamic and other solution properties of rigid proteins from atomic- and residue-level models. *Biophys. J. 101* (4), 892−8.
(62) Varea, J., Saiz, J. L., Lopez-Zumel, C., Monterroso, B., Medrano, F. J., Arrondo, J. L., Iloro, I., Laynez, J., García, J. L., and Menéndez, M. (2000) Do sequence repeats play an equivalent role in the choline-binding module of pneumococcal LytA amidase? *J. Biol. Chem. 275* (35), 26842−55.
(63) García, J. L., Díaz, E., Romero, A., and García, P. (1994) Carboxy-terminal deletion analysis of the major pneumococcal autolysin. *J. Bacteriol. 176* (13), 4066−72.
(64) López, R., García, E., García, P., and García, J. L. (1997) The pneumococcal cell wall degrading enzymes: a modular design to create new lysins? *Microb. Drug Resist. 3* (2), 199−211.
(65) Yoon, H. R., Choi, H., Choi, Y. A., Kim, J. A., Jung, J., Kim, H. M., and Jung, Y. (2018) Fabrication of Oligomeric Avidin Scaffolds for Valency-Controlled Surface Display of Functional Ligands. *Angew. Chem., Int. Ed. 57* (38), 12410−12414.
(66) Choi, S.-K. (2004) *Synthetic Multivalent Molecules: Concepts and Biomedical Applications*, Wiley-Interscience, New York (USA).
(67) Fasting, C., Schalley, C. A., Weber, M., Seitz, O., Hecht, S., Koksch, B., Dernedde, J., Graf, C., Knapp, E. W., and Haag, R. (2012) Multivalency as a chemical organization and action principle. *Angew. Chem., Int. Ed. 51* (42), 10472−98.
(68) Margni, R. A., Parma, E. A., Cerone, S., Erpelding, A., and Perdigon, G. (1983) Agglutinating and non-agglutinating antibodies in rabbits inoculated with a particulate antigen (*Salmonella typhimurium*). *Immunology 48* (2), 351−9.
(69) Bull, C. G. (1915) The Agglutination of Bacteria *in vivo*. *J. Exp. Med. 22*, 484−491.
(70) Brent, R., and Ptashne, M. (1981) Mechanism of action of the *lexA* gene product. *Proc. Natl. Acad. Sci. U. S. A. 78* (7), 4204−8.
(71) Sambrook, J., and Russell, D. W. (2001) *Molecular cloning: a laboratory manual*, Cold Spring Harbor Laboratory Press, Cold Spring Harbor, NY.
(72) Hoskins, J., Alborn, W. E., Jr., Arnold, J., Blaszczak, L. C., Burgett, S., DeHoff, B. S., Estrem, S. T., Fritz, L., Fu, D. J., Fuller, W., Geringer, C., Gilmour, R., Glass, J. S., Khoja, H., Kraft, A. R., Lagace, R. E., LeBlanc, D. J., Lee, L. N., Lefkowitz, E. J., Lu, J., Matsushima, P., McAhren, S. M., McHenney, M., McLeaster, K., Mundy, C. W., Nicas, T. I., Norris, F. H., O'Gara, M., Peery, R. B., Robertson, G. T., Rockey, P., Sun, P. M., Winkler, M. E., Yang, Y., Young-Bellido, M., Zhao, G., Zook, C. A., Baltz, R. H., Jaskunas, S. R., Rosteck, P. R., Jr., Skatrud, P. L., and Glass, J. I. (2001) Genome of the bacterium *Streptococcus pneumoniae* strain R6. *J. Bacteriol. 183* (19), 5709−17.
(73) Lacks, S., and Hotchkiss, R. D. (1960) A study of the genetic material determining an enzyme in Pneumococcus. *Biochim. Biophys. Acta 39*, 508−18.

https://dx.doi.org/10.1021/acsinfecdis.9b00344
ACS Infect. Dis. 2020, 6, 954−974

(74) Pettersen, E. F., Goddard, T. D., Huang, C. C., Couch, G. S., Greenblatt, D. M., Meng, E. C., and Ferrin, T. E. (2004) UCSF Chimera - a visualization system for exploratory research and analysis. *J. Comput. Chem. 25* (13), 1605−12.
(75) Schuck, P. (2000) Size-distribution analysis of macromolecules by sedimentation velocity ultracentrifugation and Lamm equation modeling. *Biophys. J. 78* (3), 1606−19.
(76) van Holde, K. E. (1986) *Sedimentation in Physical Biochemistry*, Prentice Hall, Inc., Englewood Cliffs, NJ, USA.
(77) Laue, T. M., Shah, B. D., Ridgeway, T. M., and Pelletier, S. L. Computer-aided interpretation of analytical sedimentation data for proteins. (1992) in *Analytical Ultracentrifugation in Biochemistry and Polymer Science* (Harding, S., Rowe, A., and Horton, J., Eds.), pp 90−125, Royal Society of Chemistry, Cambridge, UK.
(78) Guex, N., and Peitsch, M. C. (1997) SWISS-MODEL and the Swiss-PdbViewer: an environment for comparative protein modeling. *Electrophoresis 18* (15), 2714−23.
(79) Fraczkiewicz, R., and Braun, W. (1998) Exact and Efficient Analytical Calculation of the Accessible Surface Areas and Their Gradients for Macromolecules. *J. Comput. Chem. 19*, 319−333.
(80) Langmuir, I. (1916) The constitution and fundamental properties of solids and liquids. *J. Am. Chem. Soc. 38*, 2221−2295.

https://dx.doi.org/10.1021/acsinfecdis.9b00344
ACS Infect. Dis. 2020, 6, 954−974

Searching for antipneumococcal targets: Choline-binding modules as phagocytosis enhancers

Emma Roig-Molina, Manuel Sánchez-Angulo, Jana Seele, Francisco García-Asencio, Roland Nau, Jesús M. Sanz and Beatriz Maestro

Number of pages (including this one): **8**

Number of figures: **4**

Number of tables:**3**

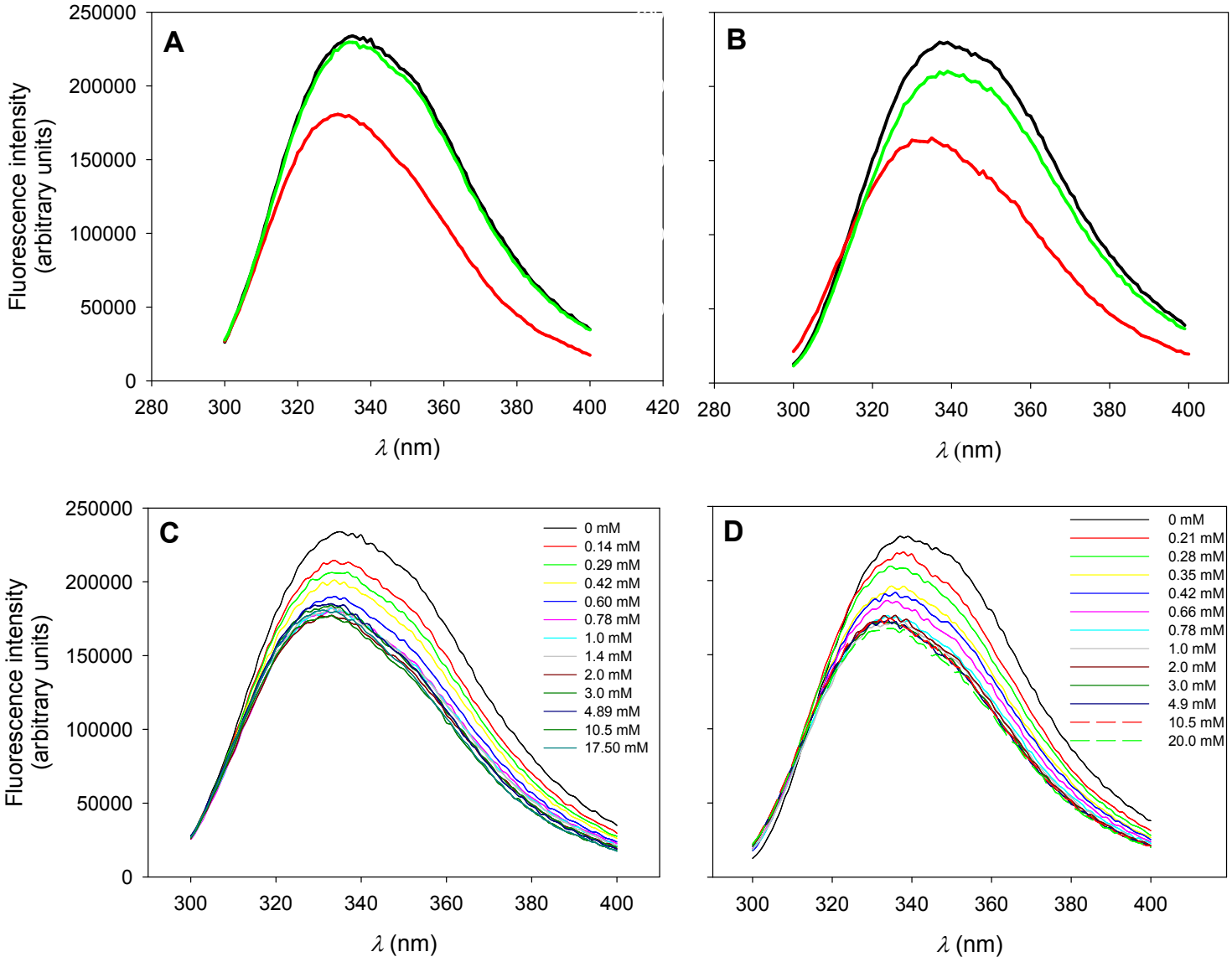

Figure S1. Intrinsic fluorescence emission spectra of C-Cpl1 (*A*) and C-CbpD (*B*) in phosphate buffer (black) plus 20 mM NaCl (green) or 20 mM choline chloride (red); Spectra registered at various choline concentrations for C-Cpl1 (*C*) and C-CbpD (*D*).

Figure S2. A planktonic culture in the stationary phase of *S. pneumoniae* R6CIB17 in the absence (left) and the presence (right) of C-LytA 1 μM

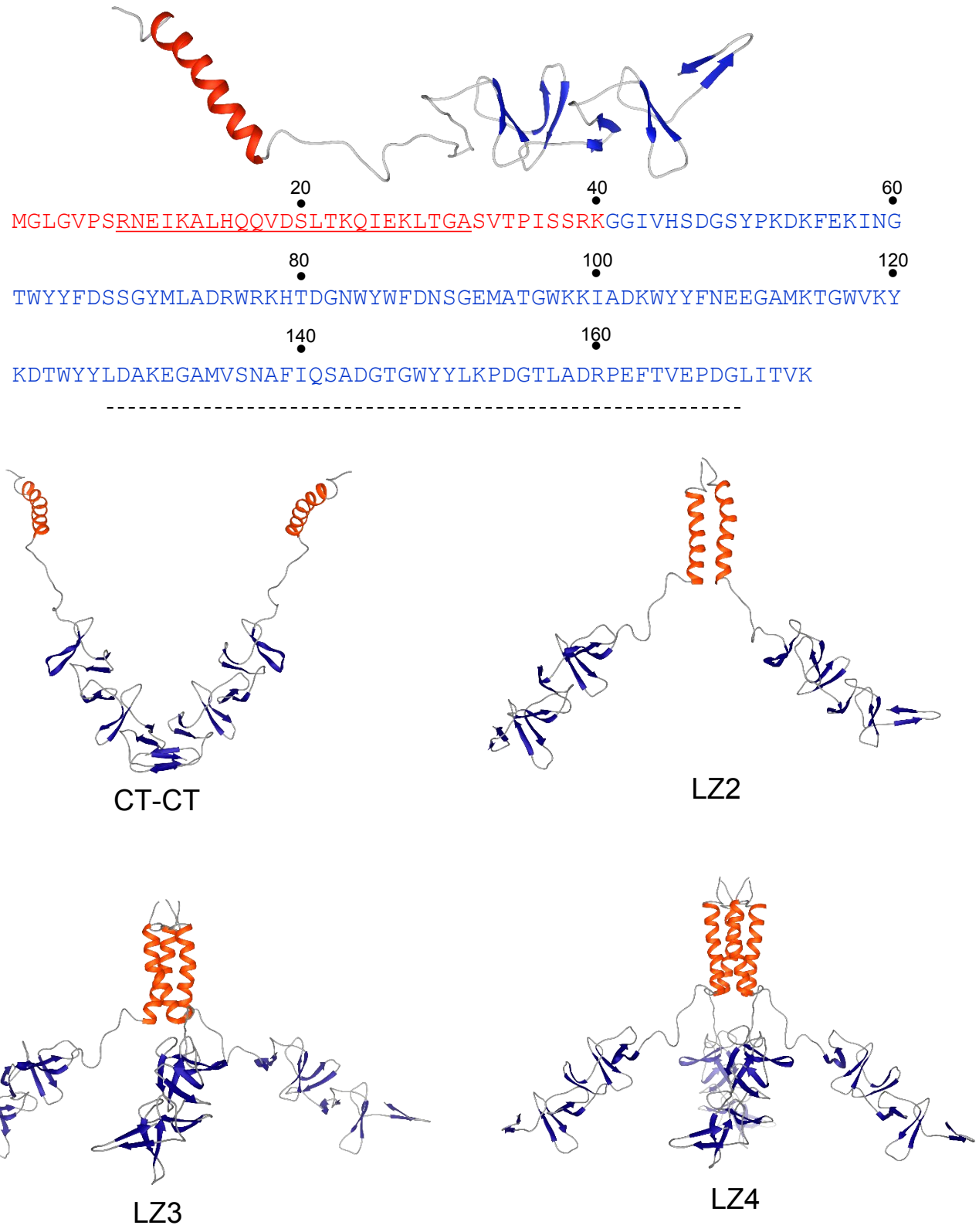

Figure S3. *Upper panel,* amino acid sequence and structural model of the monomer of the LZ-C-LytA protein. Sequence derived from the PhaF phasin is shown in blue, with the predicted leucine-zipper motif underlined. *Lower panels*: three-dimensional models of LZ-C-LytA oligomers. CT species, dimerization through the C-terminal hairpin of C-LytA; LZ species, oligomerization through the leucine zipper sequence.

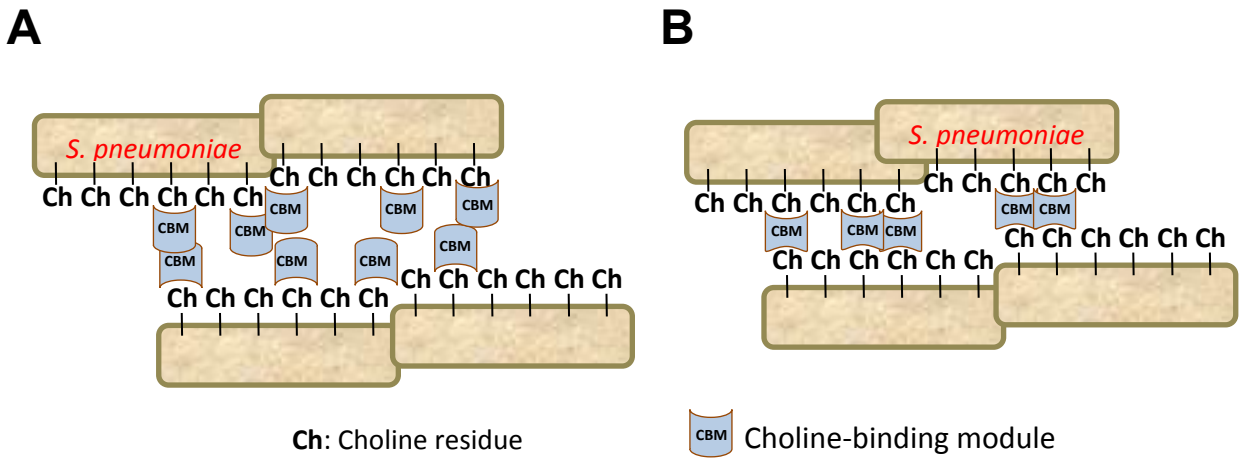

Figure S4. Possible models for CBM-induced *S. pneumoniae* agglutination. *A*, establishment of protein-protein hydrophobic interactions among CBMs adsorbed on the surface of different cells; *B*, simultaneous binding of single CBM molecules to choline residues present in different cells.

Protein	Increment in accessible surface area (ΔASA) (nm^2)		Estimation of ΔC_p (kcal mol^{-1} K^{-1})		
	Non polar	Polar	Pace[49] (Eq. 2)	Spolar *et al*[51] (Eq. 3)	Myers *et al*[50] (Eq. 4)
C-Cpl1	8025	4119	2.0	2.0	1.9
C-CbpD	5095	2558	1.2	1.3	1.2

Table S1. Theoretical estimation of ΔC_p values for C-Cpl1 and C-CbpD proteins. ΔASA values were calculated from PDB files with the GetArea utilities.[79]

Experimental sedimentation coefficient (S)	Percentage of signal (%)	Oligomeric state of model	Oligomerization mechanism[a]	Predicted sedimentation coefficient (S)[b]
1.09	3	Monomer (19899 Da)	-	1.60
2.20	27	Dimer (39781 Da)	CT2	2.31
			LZ2	2.27
2.69	64	Trimer (59662 Da)	LZ3	2.81
3.36	6	Tetramer (79543 Da)	LZ4	3.53

Table S2. Experimental and predicted sedimentation coefficients of different oligomeric modeled variants of the LZ-C-LytA protein.

[a] See Figure S4. CT species: dimerization through the C-terminal hairpin of C-LytA; LZ species, oligomerization through the leucine zipper sequence.

[b] Estimated using HydroPro utilities (see Materials and Methods)

	Protein		
	C-LytA	**C-Cpl1**	**LZ-C-LytA**
V_f (µL/min)	20	20	30
t_{as} (s)	250	350	180
t_{dis} (s)	250	350	150
Regeneration with SDS	No regeneration	0,5 %; 60 s (Three times)	0,5 %; 30 s

Table S3. Conditions of SPR experiments. *V*f, flow rate; t_{as}, association time; t_{dis}, dissociation time.